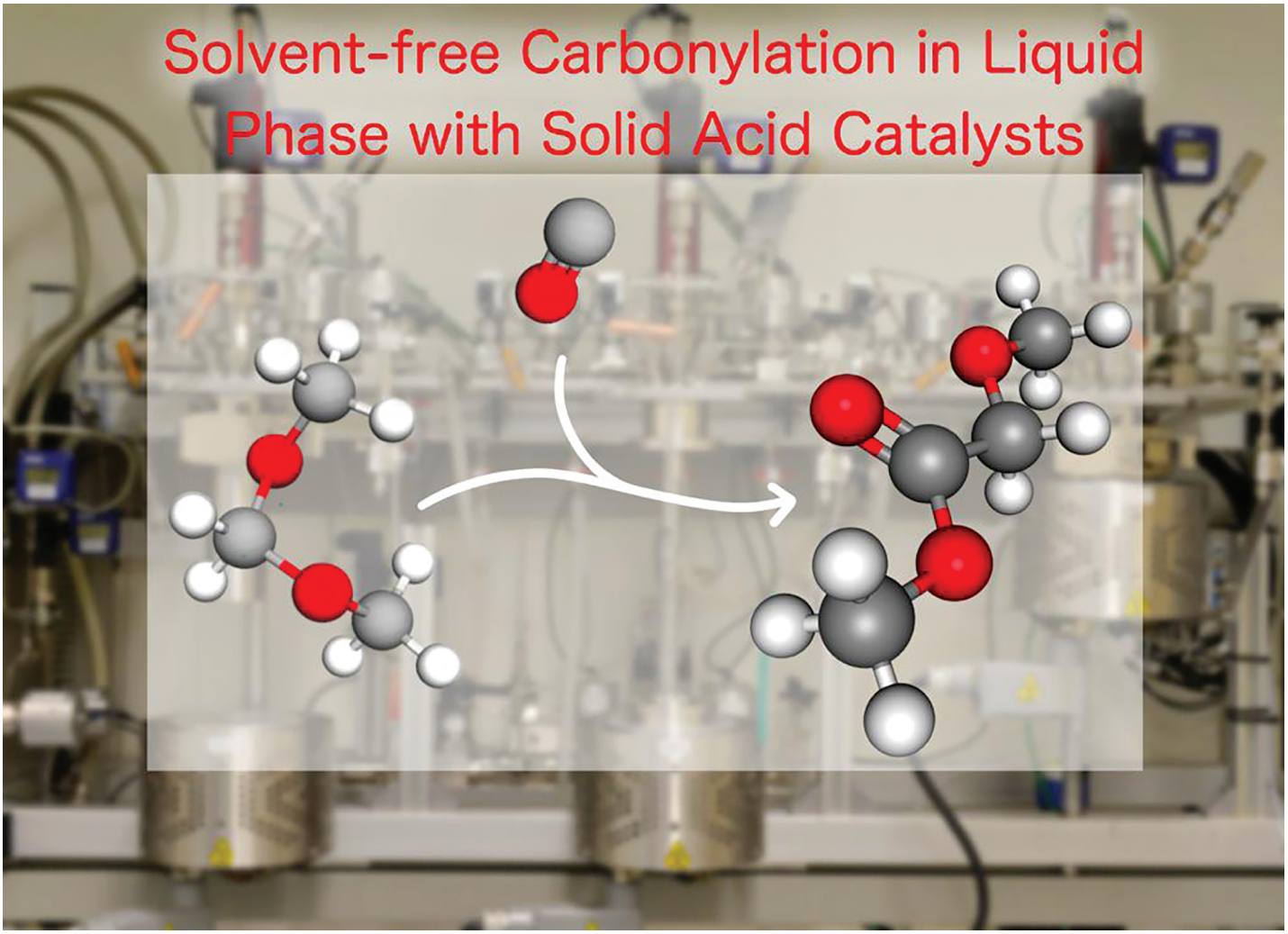

Showcasing research from Professor Sauer's laboratory, Institute of Catalysis Research and Technology, Karlsruhe Institute of Technology, Baden-Württemberg, Germany.

Carbonylation of dimethoxymethane: a study on the reactivity of different solid acid catalysts

The chemoselective, efficient, solventless carbonylation of dimethoxymethane (DMM) delivers methyl methoxyacetate (MMA), which is not only an intermediate to ethylene glycol but can also be considered as a fuel additive. Employing different zeolites and ion exchange resins as catalysts, this paper is a systematic approach to studying the effects of catalyst amount, temperature, carbon monoxide (CO) pressure and reaction conditions on educt conversion and product selectivities, using a purposely designed parallel high pressure reactor plant.

The authors would like to acknowledge Fiza A. Sheikh for the preparation of the back cover.

As featured in:

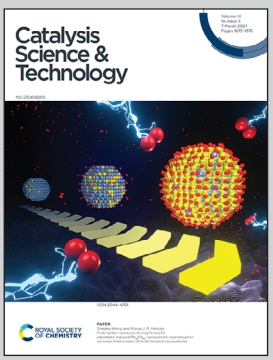

See Kalim A. Sheikh *et al.*, *Catal. Sci. Technol.*, 2024, **14**, 1148.

ROYAL SOCIETY OF CHEMISTRY

rsc.li/catalysis

Registered charity number: 207890

Catalysis Science & Technology

ROYAL SOCIETY OF CHEMISTRY

PAPER

View Article Online
View Journal | View Issue

Check for updates

Cite this: *Catal. Sci. Technol.*, 2024, **14**, 1148

Carbonylation of dimethoxymethane: a study on the reactivity of different solid acid catalysts†

Kalim A. Sheikh, * Victor Zaghini Francesconi, Thomas A. Zevaco and Jörg Sauer

Received 14th September 2023,
Accepted 10th December 2023

DOI: 10.1039/d3cy01286g

rsc.li/catalysis

The carbonylation of dimethoxymethane (DMM) to methyl methoxyacetate (MMA) has gained interest in recent years not only due to its application as an important fine chemical, but also as a possible intermediate to produce ethylene glycol (EG) as well as a possible fuel additive. Employing different zeolites and ion exchange resins as catalysts, this paper systematically studied the effects of catalyst amount, temperature, carbon monoxide (CO) pressure and reaction conditions on educt conversion and product selectivities, using a parallel high pressure reactor plant. The reaction was performed in the liquid phase without using an additional solvent. The highest DMM conversion was achieved by catalyst Z-30 (ZSM-5; MFI type zeolite) and Amberlyst 36 (sulfonated ion exchange resin). The lowest DMM conversion was shown by H-Y-30 (Y; FAU-type zeolite) and Amberlyst 46. According to the analytical measurements *via* off-line gas chromatography (GC), the product spectrum includes, besides MMA, higher oxymethylene ethers (OME) like OME_2, OME_3, the carbonylation products of higher OMEs, methyl formate (MeFo) and formaldehyde (FA). The herein reported catalysts and parameter screenings for the carbonylation of DMM to MMA will assist the optimisation of this reaction as a promising industrial manufacturing process.

1. Introduction

1.1. Application in the chemical industry

Because of the dependency of our modern civilization on limited fossil resources, much attention is being paid to finding alternative reaction pathways to synthesise different materials and products from sustainable resources. One important precursor of such compounds and reactions is methyl methoxyacetate (MMA), a fine chemical that is used in the synthesis of diverse complex organic substances. Specific applications include MMA serving as a precursor in synthesis steps of hormones,[1] of useful therapeutic substances and of organic components for biologically active substances.[2–7] MMA is also found in the synthesis of many different organic compounds, such as amino carbonyl derivatives,[8] chiral amines,[9,10] acyclic precursors to pyrroles,[11] acylation reagents for the aminolysis[12] and glycol ethers (*e.g.* ethylene glycol monomethyl ether).[13] Fig. 1 gives an overview of the aforementioned applications of MMA in the chemical industry. MMA functions as an intermediate for different organic synthesis reactions.

A further relevant commodity chemical, which can be produced from MMA, is ethylene glycol (EG), a widely employed antifreeze agent and polyester monomer. The

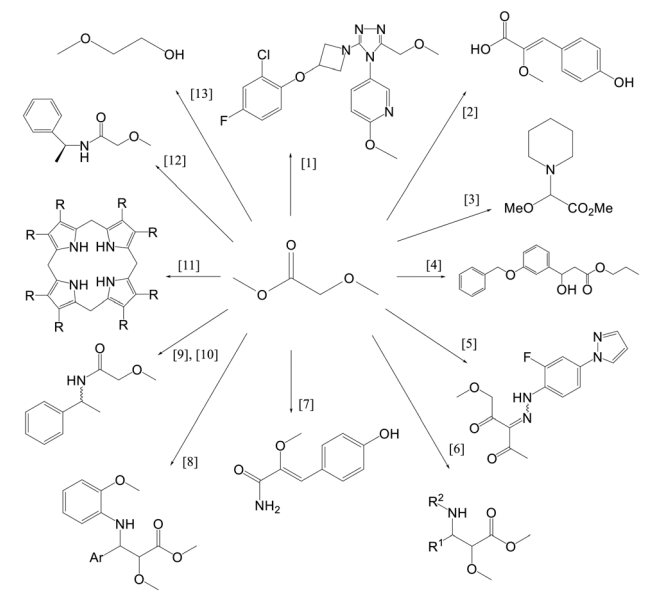

Fig. 1 Overview of different application possibilities for MMA in chemical synthesis processes; MMA functions as an intermediate for the synthesis of organic compounds. The numbers in brackets represent the literature references.

Karlsruher Institut für Technologie (KIT), Campus Nord, Institut für Katalyseforschung und –technologie (IKFT), Hermann-von-Helmholtz-Platz 1, 76344 Eggenstein Leopoldshafen, Germany. E-mail: kalim_ahmad@hotmail.de

† Electronic supplementary information (ESI) available. See DOI: https://doi.org/10.1039/d3cy01286g

manufacturing of EG is currently based on the production of ethylene from naphtha cracking, the subsequent epoxidation to ethylene oxide and a final hydration step.[14–16] Main drawbacks of this process include low yields and a complicated purification process. With increasing demand of EG, especially in China,[17,18] it is of relevance to develop sustainable routes of production.

One possible alternative is the use of syngas, preferably "environmentally friendly", gained from reverse water gas shift, as feed for the direct production of EG. However, this is coupled with high costs due to the high pressures (above 400 atm) and temperatures (above 200 °C) needed.[19,20] Another possible production route would be to use a C_1 intermediate of the syngas chemistry, such as formaldehyde (FA). This includes either the hydroformylation to glycolaldehyde or the carbonylation to glycolic acid.[16,18,21–23] The DuPont company has performed the carbonylation of FA in a commercial scale but stopped production in 1968 due to corrosion issues connected with the utilization of sulfuric acid as catalyst.[24,25] Also, high pressures are required in the process since the solubility of carbon monoxide (CO) in the solvent is low, making the process less feasible.[17] Thus the use of MMA as a precursor is a promising alternative route to EG, involving the hydrogenation of the intermediate 2-methoxyethanol and its further hydrolysis to EG.[26–30] The conventional and alternative route for EG synthesis is shown in Fig. 2.

1.2. Applications in the fuel industry

In order to reduce emissions, modern diesel engines have complex exhaust aftertreatment systems. The aftertreatment systems consists of complex catalyst systems, sensors and control units to reduce engine emissions. Therefore, instead of using such costly hardware, it would be favourable to employ new fuels or fuel additives that prevent the formation of soot and NOx within the engine, such as oxygenates like MMA.

MMA has also been reported as a possible gasoline and diesel additive.[27] In addition, Longbao *et al.*[31] described 2-methoxyethyl acetate, which has a similar structure to MMA, as an oxygenated additive of diesel to decrease exhaust emissions. Other oxygen-containing compounds, such as dimethyl carbonate (DMC),[32–35] dimethyl ether (DME)[36–38] and dimethoxymethane (DMM),[32,35,39] have also been reported as possible additives in diesel in order to reduce emissions. As an oxygenate, MMA can contribute to reduce these emissions and therefore improve diesel fuel properties.

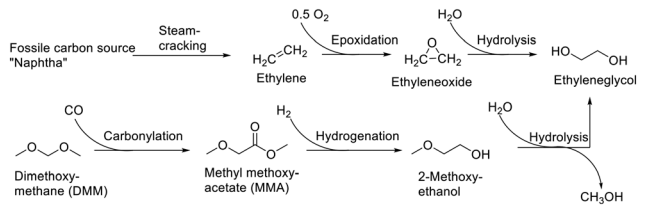

Fig. 2 Conventional and alternative route for EG synthesis.

1.3. Synthesis of MMA

Several synthesis methods to MMA have been reported in the literature, *e.g.* the reaction of methyl chloroacetate with sodium methoxide,[40] the reaction of methyl formate with FA[41,42] and the oxidation of 2-methoxyethanol.[43] These synthesis routes include complicated purification steps, are highly corrosive and are therefore unsuitable for a large-scale process. The carbonylation of dimethoxymethane presents a more attractive production route for MMA and the reaction can be carried out in the gas[44–48] as well as in the liquid phase.[26–28,49] The vapour-phase carbonylation is an easy process to be put into operation, resulting in selectivities higher than 70%.[45–48] However, the used DMM amount is small, resulting in high CO/DMM molar ratios (>100/1), which lead to low CO conversion rates (less than 0.5%).[26,27] On the other hand, the liquid phase carbonylation allows the reaction to be performed under relatively mild conditions of temperature ($T < 120$ °C) and pressure ($p < 60$ bar), leading to MMA selectivities between 50–80%.[26–28]

In this work, we report the carbonylation of DMM with CO without the use of any additional solvent, employing different commercially available catalysts, namely seven different zeolites (B-25, Y-30, F-20, M-20, Z-30, Z-80 and Z-280) and seven different ion exchange resins (Dowex 50WX2, Dowex 50WX4, Dowex 50WX8, Amberlyst 15, Amberlyst 16, Amberlyst 36 and Amberlyst 46). The influence of catalyst amount, reaction temperature, CO pressure and reaction operation were investigated.

2. Results and discussion

2.1. Catalyst screening

For an exploratory comparison of all solid acid catalysts (SAC), 10 g of DMM was introduced under argon into the autoclaves with 0.5 g of the SAC. 3550 ml of CO gas was dispensed *via* a mass-flow-controller and the mixture heated to 90 °C simultaneously (~55 bar reaction pressure). The end of the CO pressurizing was defined as the starting point of the reaction. From this point the reaction was run for 6 h. Afterwards, the gas phase was measured after cooling the reactor to room temperature. The reactor was depressurized slowly, subsequently purged with argon to evacuate residual carbon monoxide and the liquid portion was analysed using an offline-GC. Considering the ancillary character of the offline micro-GC analytics, it is not easy to directly correlate the GC results of the gas and the liquid phase and close the carbon balance. However, the gas phase analytics clearly show the role of the dissociation of DMM into DME and FA and the complexity of the reaction network.

For all performed experiments the catalytic data has been summarized as tables in the ESI† (Tables S1–S11).

2.1.1. Commercially available zeolites as SAC. The structure of the zeolites plays a central role to explain their activity in the DMM carbonylation. A wide variety of products were observed indicating a complex reaction system. The acid-catalysed decomposition of DMM to dimethylether

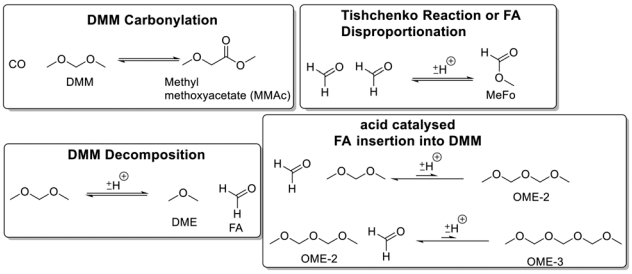

Fig. 3 Reactions observed during the carbonylation of DMM.

(DME, *i.e.* OME_0) and FA is the most prominent side-reaction in our case of study. As a matter of fact, the conversion of DMM to formaldehyde leads to valuable products. Formaldehyde being a reactive intermediate on acidic surfaces, easily undergoes Tishchenko like reactions to form methyl formate, MeFo. The aldehyde can also react with residual DMM (*i.e.* OME_1) and form higher oxymethylene ethers like OME_2 or OME_3 (see Fig. 3). The decomposition of DMM to DME is also the reason for the observed higher pressure at the end of the reaction, owing to the higher vapour pressure of DME. In comparison, the acid catalysed carbonylation of DMM to form methyl methoxyacetate, MMA, leads to a quantifiable drop of reactor pressure, allowing an accurate evaluation of the carbon monoxide conversion.

The highest catalytic activity was observed for the MFI-type (ZSM-5) zeolites as shown in Fig. 4. This widespread structure has the highest ratio of external surface to total surface area and shows, depending on the Si/Al ratio, a high Brønsted acidity. These zeolites display the highest density of Brønsted acid centres within the investigated range and inhibit efficiently the unwanted DMM decomposition (this behaviour is also observed for F-20). The MFI structure shows the higher activity towards DMM carbonylation, being the most active zeolite in the tested range. In comparison, the ferrierite (F-20) catalyst shows the highest selectivity towards higher OMEs, strongly suggesting that low SiO_2/Al_2O_3 ratio and specific pore geometry favours the insertion of FA into DMM over its decomposition to FA and DME. The FER pore geometry favours the insertion of reactive formaldehyde into already activated dimethoxymethane and higher OMEs. In comparison, the geometry and the resulting lower mobility of reactants in the pores of the H-Y-30 catalyst favours the formation of smaller molecules like methyl formate. In addition, the H-Y-30 zeolite shows the overall lowest DMM conversion, strongly suggesting that the accessibility of the acidic centres, necessary to activate the DMM for the decomposition or carbonylation reactions, is limited. The B-25 catalyst behaves quite similarly to the H-Y-30 but offers a greater porosity in general, which leads to a higher conversion level. However, the high porosity (pores volume and amount) of the B-25 catalyst leads also to an enhancement of the DMM decomposition. Z-80 and Z-280 are MFI zeolites with, regarding the Si/Al module and NH_3-TPD results, the lowest acidity from all the tested zeolite catalysts. Consequently, they do not catalyse effectively the DMM decomposition reaction to DME and show accordingly the highest pressure drop during the reaction. By contrast, Z-30 being a quite acidic zeolite, is able to decompose DMM to DME and FA. It showed, however, the highest concentration of MMA after the reaction, showing that this catalyst allows both the carbonylation and the decomposition reactions to take place. Interestingly, ferrierite F-20 shows a low pressure drop as the majority of the zeolites investigated do (for pressure curves of the screening runs see ESI† Fig. S6). This can be tentatively explained either by a low CO conversion during the reaction, not causing a measurable pressure drop, or by an intermediary state where CO consumption and DMM decomposition are kept in balance, resulting in a seemingly constant pressure. Conversion levels for most zeolites match results achieved with similar catalysts in the OME-synthesis reaction.[50]

2.1.2. Amberlyst and Dowex ion exchange resins. The screening of the ion exchange resins delivered a completely different picture regarding the DMM conversion and the

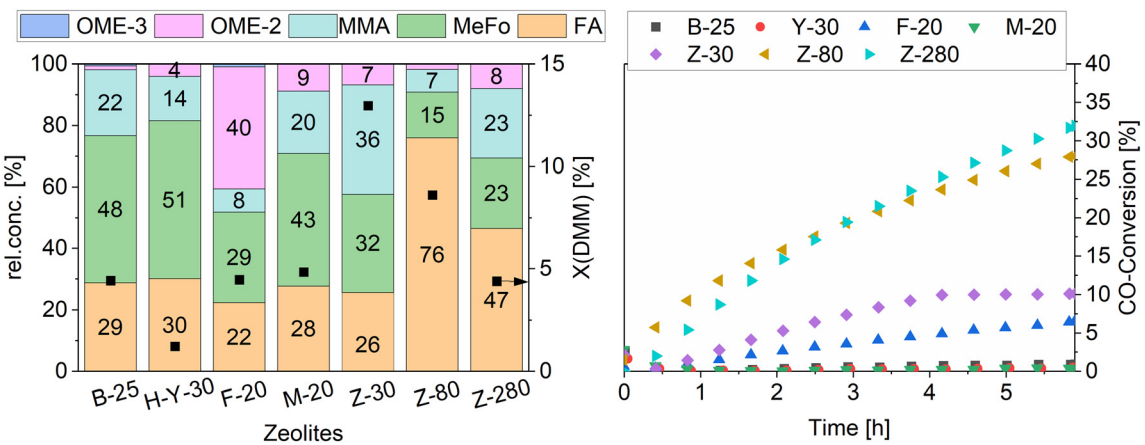

Fig. 4 Catalyst activity tests with different zeolite SAC catalysts. Performed at 90 °C, with 10 g of DMM, 0.5 g of catalyst powder, 55 bar of CO and 6 h of runtime.

relative concentrations after 6 h of reaction time. With the exception of the A46 resin, all SACs show a concentration of MMA higher than 90%, with A36 displaying the highest catalytic activity (yield 95%, selectivity 96%). Amberlyst A36 stands out as being an oversulfonated ion exchange resin, with a higher acid capacity and acid strength compared to monosulfonated catalysts with the same divinylbenzene (DVB) content.[51] In a direct comparison within the Amberlyst series, A36 has the highest acidity and acid capacity, followed by A15, A16 and finally by A46 with the lowest acid concentration (see Table 6).

Amberlyst A46 displays a particular structure, being sulfonated only at the material surface. This results in negligible amounts of acid sites in the gel phase of the polymer. Thus, most acid centres are present predominantly on the outer surface and are therefore easily accessible for catalytic reactions. Furthermore, A46 has about twice the surface area of A16 and A36, while the surface area of A15 is average when compared to the other Amberlyst catalysts (see Table 7). The formation of bulkier, *i.e.* longer-chained, products, such as higher oxymethylene ethers like OME_2, OME_3 and the carbonylation products of higher OME, are favoured with A46.

Not only the presence of sulfonated moieties plays a role in the activity of SACs, but also the DVB content has an important influence on the morphology of the catalyst, especially when employing polar media in the reaction. With a higher crosslinker content, more DVB units are linked to the styrene chains and therefore the stiffer the resin structure gets. A low DVB content usually leads to higher effects of swelling when using polar media in the reaction, creating non-permanent micro- and mesopores which can enhance the permeability of reactants.[51,52] Using linear ethers usually does not lead to a swelling of the ion exchange resins.[51,53,54] Since the reaction occurs with DMM (*i.e.* OME_1), which belongs to the oxymethylene ether chemical class, there should not be a strong swelling effect to be accounted for.

As can be seen in Fig. 6, there is a drop in DMM conversion from 28% for A15 to 22% for A16. Although A15 (4.7 mol H^+ kg^{-1}) has slightly fewer acid centres than A16 (4.8 mol H^+ kg^{-1}), it possesses a higher surface area and pore diameter, improving accessibility to active centres, which results in higher conversion rates (A15: 0.4 cm^3 g^{-1} and 300 Å; A16: 0.2 cm^3 g^{-1} and 250 Å). Compared to A16, the DMM conversion of A36 more than doubles to reach a value of 55%. Since A16 and A36 have similar surface areas and pore diameters, the difference in reactivity can be mainly explained by the higher concentration of acid sites on A36 (5.4 mol H^+ kg^{-1}), as well as by the oversulfonation of the polymer in A36. The catalyst A46 shows a different conversion and selectivity pattern when compared to the other ion exchange resins. DMM conversion lies below 7% with a relative MMA concentration of just 38%. A46 has the highest surface area among the Amberlyst catalysts and a pore diameter similar to A16 and A36. However, with the smallest concentration of acid sites (0.43 mol H^+ kg^{-1}), it demonstrates the importance of the materials' acidity in the conversion of DMM to MMA.

The importance of availability and accessibility of acid sites in such ion exchange resins is also supported by the results obtained with the Dowex catalysts. This catalyst class shows a similar selectivity towards MMA, higher than 90%, even though there are some differences in the acid sites concentration.

Dowex catalysts are gel-type resins. The terminal number of the Dowex catalyst series describes the divinylbenzene content (2%, 4% and 8%), which is a measure for the degree of cross-linking of the polystyrene backbone. Catalysts with a more strongly cross-linked matrix might show reduced activity due to the stiffness of the catalyst and therefore a more difficult accessibility of the active acidic centres. However, this is not what is seen in the presented results, as seen in Fig. 6. When analysing the results from the Amberlyst series, the DVB content does not correlate with the conversion and selectivities of the catalyst. A15 and A46 present the highest amount of crosslinkers, but do not show the highest catalytic activity. Therefore, when comparing to the Dowex catalysts, the amount of crosslinker cannot be the catalyst property responsible for the different conversion levels observed. In addition, the surface area is in the same order of magnitude for all Dowex catalysts employed in this study. This leads to the conclusion that the concentration of acid sites and their accessibility in a porous polymer matrix represents the major factor to explain the difference in DMM conversion. DX2 shows a DMM conversion of 25% (3.68 mol H^+ kg^{-1}), while DX8 has a DMM conversion of 40% (4.51 mol H^+ kg^{-1}), demonstrating the major effect of acid site capacity. As described before, the accessibility to the catalytic active centres plays a central role in the reaction to bulkier products and therefore the selectivity to higher oxymethylene ethers like OME_2, OME_3, as well as the carbonylation products of higher OME. The product selectivities for the Dowex series are not largely affected by the different DVB content and different acid site concentrations. Other morphological aspects, such as the surface area, have a higher influence on the MMA selectivity. These characteristics have similar values for the used Dowex catalysts, resulting in an overall similar product spectrum with a MMA selectivity higher than 90%.

The A36 SAC is not only the most active, but also the most selective catalyst used in this study. Regarding all ion exchange resins at 90 °C after 6 h, it exhibits the highest conversion for CO with nearly 30%. All ion exchange resins also catalyse the DMM decomposition, but not enough DME had been formed to be measured after the reaction. In contrast to the zeolites (excluding Z-30), also a carbonylation of higher OMEs was observed yielding the corresponding esters (see Fig. 5). Multiple CO insertions into one molecule of OME_2 and OME_3 were also observed (see ESI† Fig. S1).

2.1.3. Structure–reactivity relationships for zeolites. The interpretation of the data from the zeolites appears to be more complex. All characterization data for zeolites discussed here will be presented in the experimental part of this publication. The product spectrum of each zeolite is quite different from one another, making a comparison and

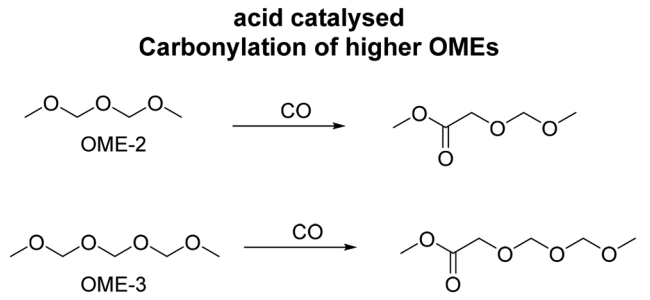

Fig. 5 Carbonylation of higher OMEs yielding the corresponding ethers.

discussion of the results not trivial. The extremes of the catalysts' properties do not necessarily translate in an immediate effect or trend on the reaction process, *i.e.* a very high acid site density or a very high acidity does not showcase itself clearly in form of a higher conversion or specific product selectivity. In addition, even comparing zeolites with similar properties does not lead to clear tendencies for the reactivity of the carbonylation of DMM.

Y-30 has the highest BET surface area (879 m^2 g^{-1}) and comparatively high values for pore volume (0.204 cm^3 g^{-1}), the pore diameter lies within the range of the other tested zeolites (3.896 nm). B-25 has a moderately high BET surface area (602 m^2 g^{-1}) and the highest pore volume (0.570 cm^3 g^{-1}) and pore diameter (6.789 nm). All the other zeolites show significant lower values of these before mentioned properties and similar values overall (see Table 8).

Considering the catalytic properties of acid site density and strength, both catalysts B-25 and Y-30 show relatively similar values (see Table 9). Considering acid strength, more than two-third of the sites of both catalysts are regarded as strong or very strong (77% and 86%, respectively). In regard to the NH_3 uptake, which correlates to the acid site density, B-25 has almost double the NH_3 uptake (596.55 μmol g^{-1}) than Y-30 (320.02 μmol g^{-1}). For both of these catalysts, the selectivity for FA and MeFo are similar and the MMA selectivity is also in a similar range. The CO conversion is similarly low, but the conversion for DMM lies quite apart. The B-25 catalyst with its higher pore volume and diameter, as well as higher acid density, shows a slightly higher DMM conversion. The conversion for both reactants is low, however.

The catalysts F-20 and M-20 have a similar DMM conversion but very different CO conversion and product selectivities. F-20 has the highest NH_3 uptake (1065.8 μmol g^{-1}), *i.e.* high acid density; half of the acid sites are considered weak sites (44%) and the other half either strong or very strong (56%). M-20 has a slightly lower acid density (836.15 μmol g^{-1}) but a higher amount of strong or very strong acid sites (77%). This property constellation for F-20 results in very high amounts of OME_2 (40%) and one of the lowest percentages of the desired product MMA (8%). M-20 has a slightly higher DMM conversion, a very low CO conversion and a higher MMA concentration (20%), but also high amounts of FA (28%), MeFo (43%) and OME_2 (9%).

B-25 and Z-30 have similar acid site densities (596.55 and 608.91 μmol g^{-1}), however very distinct DMM conversions (4 and 13%), CO conversions (1 and 10%) and MMA selectivity (22 and 36%). This difference can tentatively be explained by the different acid strength. Z-30 is the catalyst with the weakest acidity, with 65% of the acid sites being regarded as weak. This leads to a lesser decomposition of DMM and a higher selectivity for the carbonylation reaction.

Comparing zeolites with similar acid strength also leads to no clear tendency among the catalysts, *e.g.* when comparing B-25, M-20, Z-80 and Z-280, all having 72–77% strong or very strong acid sites. Each catalyst presents a very different DMM conversion (4–9%), CO conversion (0.4–32%) and MMA selectivity (7–23%). B-25 and M-20 have very similar conversion levels and product selectivities. Both have similar BET surface areas and similar acid strengths, with slightly different acid sites density. The pore structure is quite different (diameter, volume and surface area). Thus, the acid sites strength seems to have the highest impact on product selectivity and conversion.

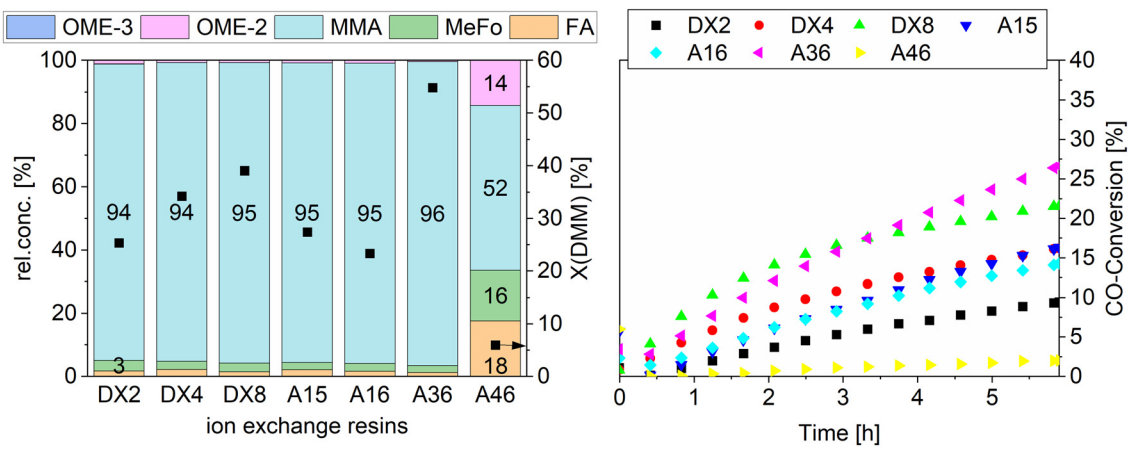

Fig. 6 Catalyst activity tests with different ion exchange resins SAC catalysts. Performed at 90 °C, with 10 g of DMM, 0.5 g of catalyst, 55 bar of CO and 6 h of runtime.

When comparing catalysts from the same morphological structure, as Z-30, Z-80 and Z-280, one can only see a clear trend in the DMM conversion. Z-30 shows the highest DMM conversion (13%) and MMA selectivity (36%) among all zeolites. Z-30 shows a moderate acid density (608.91 μmol g^{-1}) and the highest amount of weak acid sites among the zeolites (65%). This set of properties seems to favour the carbonylation and less the decomposition of DMM. The catalysts Z-80 and Z-280 have the lowest acid site density (317.07 and 65.67 μmol g^{-1}) and a very similar acid site strength (72 and 75% are regarded as strong or very strong sites); they demonstrate a reduced DMM conversion level but the highest tendency for DMM decomposition (76 and 47% FA). The MMA concentration is relatively low (7 and 23%).

From the gathered data for the zeolites, a low to moderate acid site density and a tendency for weak acid sites seems to be the best compromise for a moderate DMM conversion (13%) and MMA selectivity (36%), as seen in Z-30. B-25 with its highly accessible pore structure and Y-30 with its high BET-surface area do not show a direct effect on the reactivity for the carbonylation. In this regard, the acid site density and strength seem to have a higher impact (Table 1).

2.1.4. Structure–reactivity relationships for ion exchange resins. In a direct comparison with the ion exchange resins, a clear difference in reactivity between zeolites and ion exchange resins is seen. The conversion levels for DMM and selectivities towards MMA are much higher. Thus, ion exchange resins are the more promising catalysts for the efficient DMM carbonylation reaction towards MMA.

All characterization data for the resins discussed here will be presented in the experimental part of this publication. Comparing the data from the experiments with the Amberlyst and Dowex catalysts, we can infer a few evaluations. For the ion exchange resins, the conversion and selectivity levels are very similar, with two exceptions, namely A36 (showcasing a significant higher DMM conversion) and A46 (showcasing a comparatively low DMM conversion and different product spectrum).

The main difference of A46 when compared to the other resins is the fact that it is only surface sulfonated. This translates in a high accessibility of acid sites, but at the same time a lower acid capacity by a factor of 10, which in turn renders a lower catalytic activity (see Table 6). The lower catalytic activity in regard to the carbonylation of DMM to MMA leads to the possibility of different reaction pathways, such as side reactions as DMM decomposition. This leads to build-up of formaldehyde, following up with formation of MeFo and formaldehyde insertion in DMM to higher oxymethylene ethers. Additionally, the sulfonation degree plays an important role for the conversion level of the ion exchange resins. This can be seen by a direct comparison of A16 and A36, which are part of the same catalyst family, but one being monosulfonated (A16, having about one $-SO_3H$ group per aromatic ring) and the other being oversulfonated (A36, having between 1 and 1.2 $-SO_3H$ groups per aromatic ring).[51] Here, there is a clear difference in the DMM conversion, with A36 showing a more than doubled DMM conversion value when compared to A16. The catalyst A15 has a slightly lower acid capacity than A16, but a higher accessibility of acid sites, indicated with a higher surface area, pore diameter and pore volume. This would be a possible explanation for the slightly higher DMM conversion of A15.

The Dowex catalysts have a comparatively small surface area and pore diameter since gel type resins generally do not feature measurable porosity when dry.[55–57] Their acid capacity is comparable to the Amberlyst catalysts, though. When comparing the Dowex catalysts among themselves, apart from the DVB-content (crosslinker), the main difference between them lies in the acid capacity; the higher the capacity, the higher the conversion, without influence on the product spectrum. As discussed earlier (section 2.1.2), swelling of the resins is not expected, since DMM does not induce this phenomenon. Therefore, the DVB-content does not play a major role in the reactivity of the carbonylation of DMM in the liquid phase.

The fact that the crosslinker content and the acid site accessibility (surface area, pore volume and pore diameter) do not have a major impact on the reactivity and the fact that the formation of bulkier molecules, such as higher oxymethylene ethers, only happened with A46, suggests that the DMM carbonylation mainly takes place on the surface of the catalysts and less on the resin gel-phase. The acid capacity and sulfonation degree are the most important catalyst properties to determine the product spectrum and conversion. This is especially the case because no swelling of the resins is expected.

For a selection of the proper ion exchange catalyst for the DMM carbonylation, one should consider 2 important aspects: acid capacity and further important morphological aspects, *e.g.* sulfonation degree.

Considering all aspects, A36 presents the most promising catalyst, showing the highest acid site concentration, an oversulfonated structure and a good acid site accessibility, resulting in high MMA selectivity and high DMM and CO conversions already at low temperatures. The A36 catalyst showcased a DMM conversion of 55% and MMA concentration of 96%. Since A36 has proved to be the catalyst with the highest activity and selectivity, it was used for further studies of this catalytic reaction. To further

Table 1 Comparison of the catalytic results for the zeolites in contrast to the structural property of the NH_3 uptake

Catalyst	*S*(MeFo) [%]	*S*(MMA) [%]	*X*(DMM) [%]	*X*(CO) [%]	NH_3 uptake [μmol g^{-1}]
B-25	47.78	21.57	4.44	0.91	596.55
H-Y-30	51.46	14.42	1.22	0.52	320.02
F-20	29.42	7.61	4.48	6.54	1065.8
M-20	43.00	20.32	4.85	0.39	836.15
Z-30	31.84	35.60	12.97	10.14	608.91
Z-80	14.96	7.31	8.61	27.89	317.07
Z-280	22.91	22.64	4.40	31.69	65.67

Table 2 Comparison of the catalytic results for the resins in contrast to the structural property of the capacity in the dry state

Catalyst	S(MeFo) [%]	S(MMA) [%]	X(DMM) [%]	X(CO) [%]	Capacity (dry) [mol H^+ kg^{-1}]
DX2	3.37	93.72	25.38	9.45	3.68[b]
DX4	2.60	94.42	34.26	16.21	4.47[b]
DX8	2.76	95.01	39.06	21.58	4.51[b]
A15	2.31	94.80	27.43	16.34	4.7[a]
A16	2.49	94.96	23.36	14.32	4.8[a]
A36	2.12	96.10	54.84	26.61	5.4[a]
A46	15.98	52.15	5.95	2.00	0.43[a]

[a] Manufacturer's data. [b] Value derived from manufacturer's data.

understand the reaction, a broad parameter study was conducted by variation of catalyst amount, temperature, pressure and reaction operation (Table 2).

2.2. Parameter studies performed with Amberlyst 36

2.2.1. Effect of catalyst amount. The amount of DMM was changed to 43 g (50 ml) and the pressure in the reactors was kept constant by compensating the CO consumed during the reaction. This leads to a nearly complete DMM conversion despite the limited gas phase in the reactors and to an easy monitoring of the reaction over a longer reaction time.

The first study was conducted at 110 °C and the catalyst amount was varied between 0.5, 1 and 1.5 g of A36. The results are shown in Fig. 7. After the first hour, the difference in the relative concentrations is negligible between the different catalyst amounts. The DMM conversion is lower for the 0.5 g run compared to the 1 g or 1.5 g runs, which show similar DMM conversions. After 4 h and 6 h the difference in DMM conversions becomes noticeable between the 1 and 1.5 g run. This hints towards the fact that the amount of active species is important for the faster DMM conversion, but not influencing the selectivity of this reaction. Other products like methyl formate, formaldehyde and higher OMEs are only measured as traces. The CO conversion confirms what is also observed by evaluating the DMM conversion and relative concentration results. With 0.5 g of catalyst, the equilibrium CO conversion is not reached in 6 h. By contrast, the equilibrium conversion for the 1 g and 1.5 g run is reached nearly at the same rate (Fig. 8). One should keep in mind that DME is a side product in this reaction. The DME formation could only be compared between these three runs and showed only a small increase from 0.5 to 1.5 g. For future studies, 1 g of A36 was chosen as the benchmark amount yielding fast DMM conversions to properly follow the reaction progress.

2.2.2. Effect of temperature. A broad temperature variation was conducted using the A36 catalyst. We chose seven temperatures ranging from 40 to 140 °C, the reaction being monitored after 3 h (data for liquid samples taken at different times can be found in the ESI† in Tables S5–S7). The results from the temperature variation are presented in Fig. 9. Increasing temperature leads clearly to the decomposition of DMM, becoming a major side reaction and generating more DME with concomitant increase of the pressure and decrease of the CO conversion. Moreover, at temperatures higher than 110 °C the A36 catalyst started showing a strong leaching, leading to a yellowish substance. Ion exchange resins are generally unstable at higher temperatures and break down into low molecular weight sulfonic acids.[58,59] These tend to be much better soluble in organic solvents and leads to a leaching of the SACs into the liquid phase, making this reaction predominantly homogenously catalysed.[60] This effect becomes stronger the

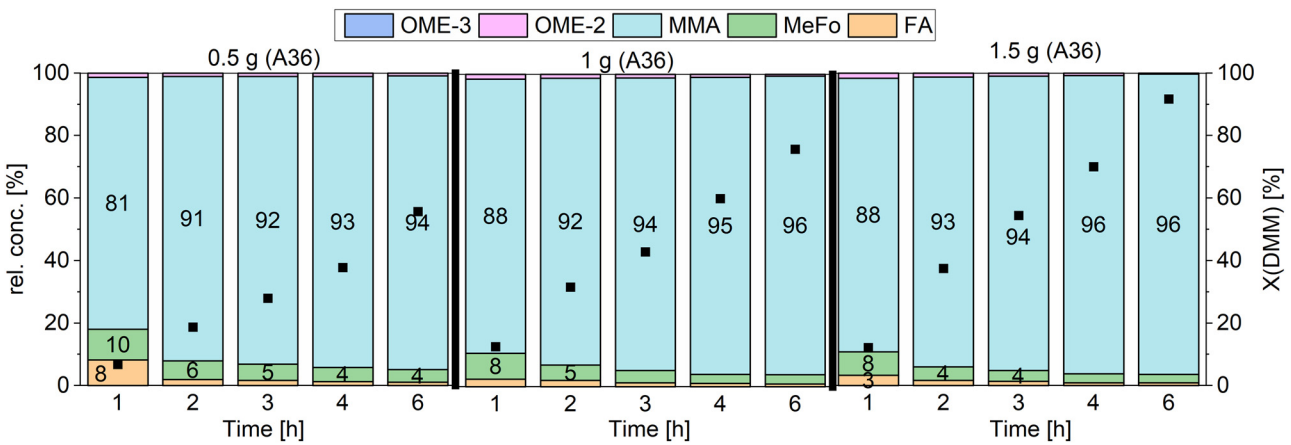

Fig. 7 The effect of variation of catalyst amount on the relative concentrations of the products and the DMM conversion.

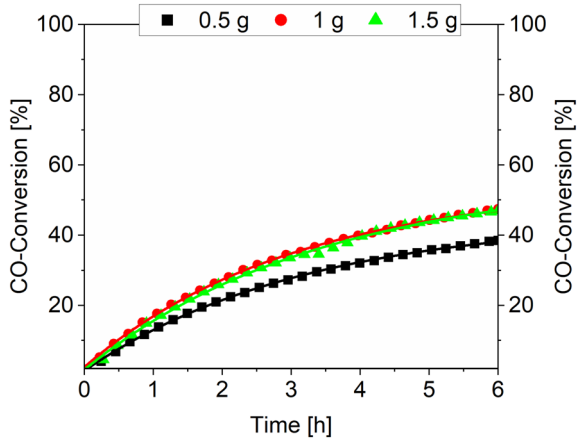

Fig. 8 The effect of variation of catalyst amount on the CO conversion calculated from the pressure drop in the reactor.

higher the temperatures get and was not specifically quantified in this work. In order to suppress the decomposition of the products, a milder temperature around 100 to 110 °C is needed, which allows a sufficiently high reaction rate, without degradation of the catalyst. The CO conversion rate and the DMM conversion rate again match very well and show that the highest CO equilibrium conversion can be reached at 120 °C. Performing in the 110–120 °C region leads to high conversions for CO and DMM in a short reaction time (3 h). CO conversion for these milder temperatures is nearly equal to the pressure drop in the reactor because nearly no DME is formed, but the overall reaction rate is rather slow. Low temperatures increase the catalyst lifetime, but the residence time of the reactants has to be increased to achieve comparable reaction rates.

2.2.3. Effect of pressure. Fig. 10 shows the comparison of the catalytic activity of A36 at different pressure levels (20, 40, 60 and 80 bar). The reaction was conducted at constant pressure by compensating the consumed amount of carbon monoxide under reaction conditions. A nearly linear increase of the DMM conversion was observed, while the slope of the graph is dependant on the pressure. Interestingly, the highest conversion of DMM after 1 h was observed at 60 bar. Further increasing the pressure to 80 bar did not have a high impact on the DMM conversion. Comparing the DME content in the gas phase after all 4 runs shows a remarkable trend. The formation of DME increases the overall pressure of the system, due to the partial pressure of DME being higher than that of DMM or MMA. Both competing reactions cancel out the effect on the pressure. The DME formation increases, whereas the MMA formation decreases the reactor pressure. The pressure drop is correlated to MMA formation and concurrent CO conversion and also to the substantial difference in partial pressure of MMA and DMM at 110 °C. This efficient carbonylation of DMM leads to MMA becoming the major component of the liquid phase already after 3 h of reaction time, performing the reaction at 60 and 80 bar (see Fig. 10). Conversely, performing the reaction at a constant pressure of 20 bar leads to an increased DMM decomposition to form DME and FA. This demonstrates nicely the effect of the Le Chatelier principle, the pressure in the reactor being too low to repress the formation of DME. FA cannot stay under the experimental conditions in its molecular form and undergo both a disproportionation reaction to MeFo and (even though less likely) an insertion into DMM to form higher OMEs. This effect can be clearly observed in the pressure diagram for all 4 experiments in Fig. 11. The continuous dosing of CO was programmed so that the automated dosing procedure starts when 2 bar of the reactor pressure has been consumed by the reaction, filling the reactor back to the initial pressure. It is clearly visible that the time intervals between the re-pressurizing steps become smaller the higher the reaction pressure is. Furthermore, the time intervals observed in the CO replenishing procedure become larger, the longer the reaction proceeds.

2.3. Fuel properties

In order to evaluate the potential of MMA as a diesel fuel alternative or additive, relevant physico-chemical and fuel properties were analysed and are displayed in Table 3. The data for MMA, OME_{3-5} and diesel (EN 590) were compared. The OME_{3-5} fraction also belongs to the substance class of the

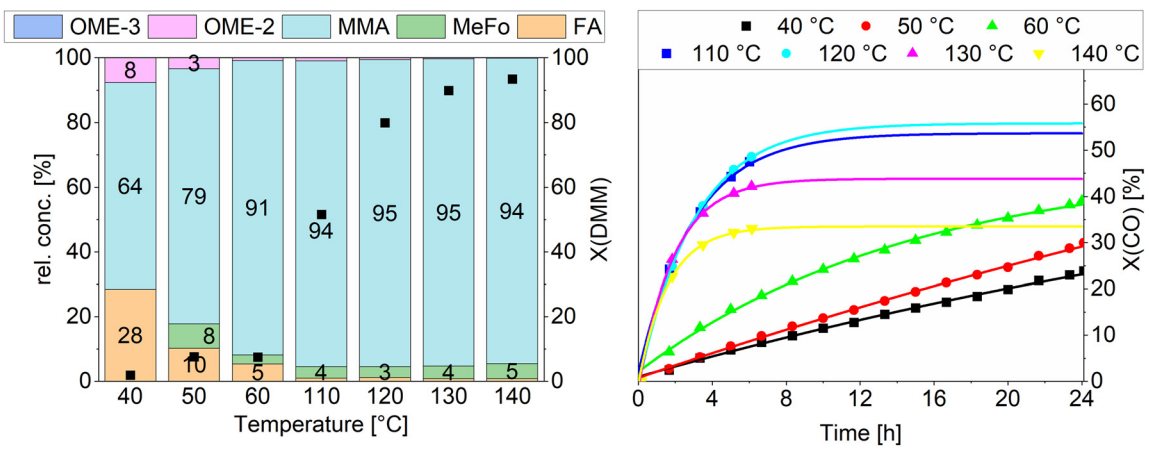

Fig. 9 The effect of temperature on the CO conversion rate.

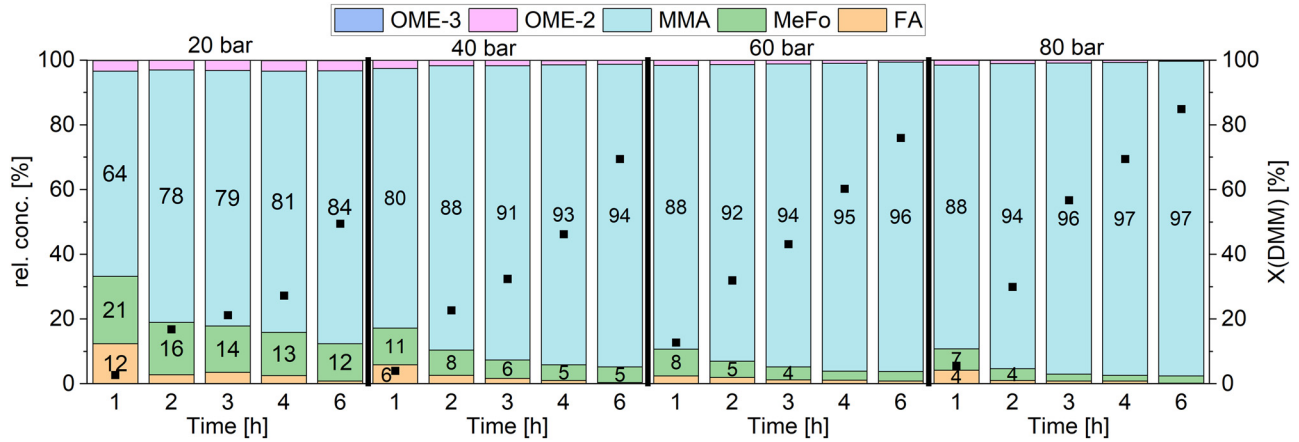

Fig. 10 The effect of reaction pressure at the relative concentrations of the products and the DMM conversions for different reaction times. Reaction conditions: 110 °C, 1 g of A36 and constant pressure of CO.

oxygenates and is widely discussed as an alternative diesel fuel.[32,61–63] For sake of comparison, it was also included in Table 3.

The cetane number describes the ignitability of a diesel fuel. The higher it is, the easier it is for the fuel to ignite. Since the diesel engine works without spark ignition, the fuel must be able to self-ignite when injected into the hot, compressed air in the combustion chamber. Hence the necessary high cetane number above 51 for commercial diesel fuels. A flash point above 55 °C is important for safety reasons during transportation and storage. The flash point is the temperature at which a flammable liquid will release enough vapour into the surrounding air that an ignition source can ignite the air/vapour mixture above the liquid. The viscosity is a measure of the resistance during the flow of a fluid due to internal friction. If the viscosity of the diesel fuel is too low, it leads to increased leakage losses in the injection pump and thus to a worse engine performance. By comparing the properties of MMA with those of diesel fuel (Table 3), there are a few characteristics which make MMA more appropriate as a fuel blending component rather than as a diesel fuel replacement.

The flash point of 42 °C (diesel: >55 °C), the cetane number of 14.4 (diesel: ≥51) and the viscosity of 0.75 (diesel: 2–4.5) are lower than the values stipulated by the diesel standard EN 590. The autoignition temperature of 350 °C is within the range of the standard. The lubricity seems comparable to diesel, but due to a quick evaporation of the sample at 60 °C, the parameter could only be measured at 25 °C. The heating value of MMA is roughly half of fossil diesel, which is a common trait of oxygenates due to an inherent high oxygen content. The density of MMA is higher than diesel fuel but comparable to other oxygenates, such as OME. The low cold filter plugging point (CFPP) value of −70 °C and low melting point of −38.7 °C of MMA could improve cold stability properties of a diesel–MMA fuel blend.

As can be inferred from the comparison of the characteristics with fossil diesel, MMA does not fulfil the criteria for a diesel fuel replacement. However, as an oxygenate, MMA clearly represents a possible diesel fuel additive, considering the high soot and NOx reduction potential. This is in line with more general studies with oxygenates that an oxygen content of about 10–20 wt% in the fuel blend (*e.g.* with diesel) would be sufficient for an extensive reduction of soot emissions.[32,34,35,61–63,65–67]

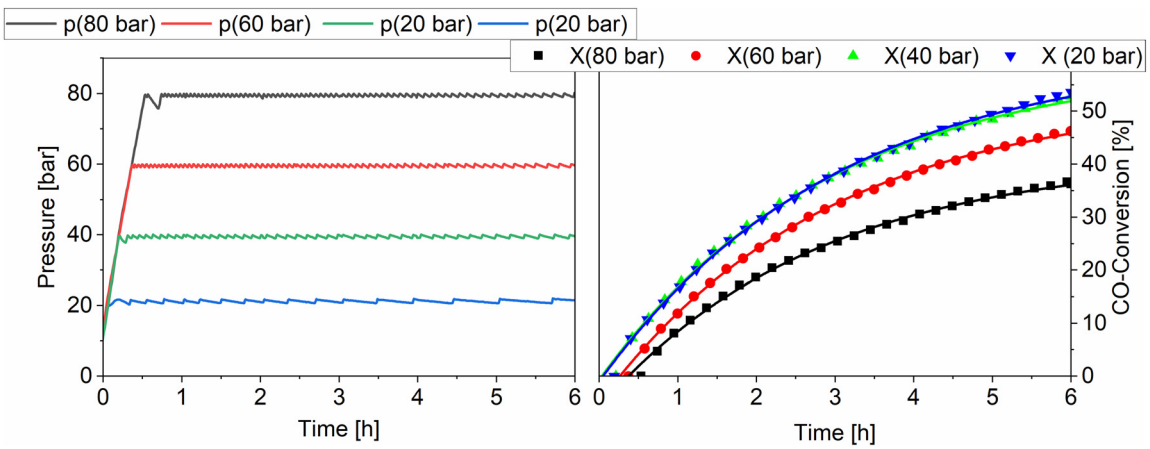

Fig. 11 The effect of pressure on the CO conversion rate calculated by the pressure drop in between redosing of CO.

Table 3 Physico-chemical and fuel properties of MMA, OME_{3-5} (as another oxygenate as potential alternative diesel fuel) and diesel (EN 590)

Test parameter	Test method/source	MMA	OME_{3-5}[a]	Diesel (EN 590)[b]	Unit
Melting point	ASTM D5972: 2016	−38.7	−43 (OME_3) −10 (OME_4) 18 (OME_5)	Not specified	°C
Refractive index (20 °C)	DIN 51423-2: 2010	1.3969	1.396 (OME_3) 1.406 (OME_4) 1.413 (OME_5)	Not specified	—
Surface tension (20 °C)	DIN EN 14370: 2004	32.3	28.8 (OME_3) 30.7 (OME_4) 32.6 (OME_5)	Not specified	mN m^{-1}
Flash point	DIN EN ISO 3679: 2015	42.0	54 (OME_3) 88 (OME_4) 115 (OME_5)	>55	°C
Autoignition point	DIN 51794: 2003	350	235 (OME_3) 235 (OME_4) 240 (OME_5)	≥220	°C
Cetane number	DIN EN 17155: 2018	14.4	72 (OME_3) 84 (OME_4) 93 (OME_5)	≥51	—
CFPP	DIN EN 116: 2018	−70	−38 (OME_{3-5} mixture)	Time-dependent (5 to −20 °C)	°C
HFRR (lubricity at 60 °C)	DIN EN ISO 12156-1: 2019	420 (25 °C)[c]	534 (OME_3) 465 (OME_4) 437 (OME_5)	<460	μm
Heating value	In-house analytics	20.559	19.6 (OME_3) 19.0 (OME_4) 18.5 (OME_5)	43	MJ kg^{-1}
Density (15 °C)	In-house analytics	1.0584	1.0305 (OME_3) 1.0737 (OME_4) 1.1057 (OME_5)	0.815–0.845	kg l^{-1}
Kinematic viscosity (40 °C)	In-house analytics	0.75	1.08 (OME_3) 1.72 (OME_4) 2.63 (OME_5) (25 °C)	2–4.5	mm^2 s^{-1}

[a] Values from Lautenschütz *et al.*[62] and Arias *et al.*[64] [b] Parameters considered only for winter diesel in temperate climatic zones (not in arctic climate zones). [c] Parameter measured at 25 °C due to evaporation of sample at 60 °C.

Also, the good cold stability properties of MMA could be beneficial in a diesel–MMA blend.

Due to its low cetane number of 14.4 (see Table 3), MMA also shows potential as a possible gasoline additive or alternative. For gasoline, an important fuel property is the research octane number (RON), which describes the ability of the fuel to withstand compression in an internal combustion engine without igniting. For this type of engine, a spark ignition at the end of the compression stroke is needed. Generally speaking, diesel fuels have a high cetane number >40 and a small RON < 40; by contrast, gasoline fuels have a low cetane number <19 and a high RON > 90.[68] According to correlations between cetane number and RON, MMA should present a RON above 95,[69,70] matching the European fuel specifications regarding this fuel property.[71]

3. Materials and methods

3.1. Materials and experimental procedures

Chemicals: chemicals and materials were supplied by Merck KGaA[M], Air Liquide[AL] and Thermo Scientific[TS] and used without further purification. The values in brackets show the purity and other properties.

Carbon monoxide (99.97%, 200 bar, 40 l)[AL], argon (99.9999%, 200 bar, 50 l)[AL], dimethoxymethan (≥99.50%)[TS], methyl methoxyacetate (≥99%)[TS], methyl formate (≥97%)[TS], *p*-formaldehyde (≥95.0%)[M], methanol (99.8%, extra dry over molecular sieves)[TS], OME_2 and OME_3 (≥95.0%) were synthesised and purified according to the procedure described by Lautenschütz *et al.*[72] The commercially available zeolite powders were all used as received from Zeolyst International, the product information given by the manufacturer is shown in Table 4. The ion exchange resins are commercially available strongly acidic catalysts from Rohm & Haas and Dow Chemical. They were dried for 12 h at 110 °C under reduced pressure (p < 10 mbar) before usage. An overview of the ion exchange resins tested in this study is shown in Table 5.

Catalyst testing and apparatus: catalyst testing procedure has been described elsewhere,[73] but was slightly modified for the experiments described in this work. A plant equipped with three parallel high pressure autoclaves for screening of catalytic reactions (PASCAR: PArallel Screening of CAtalytic Reactions; standard operational conditions: P_{max}: 175 bar, T_{max}: 200 °C, reactor volume: 100 ml, Premex mechanical stirrer, liquid probe sampling *via* definite tubing loop) was

Table 4 Overview of the product information for the zeolyst catalysts

Product code ZEOLYST	SiO_2/Al_2O_3 ratio	Cation	Na_2O [wt%]	Surface area [$m^2\ g^{-1}$]
Y-Type zeolite powder (FAU)				
CBV 720	30	Proton	0.03	780
Mordenite type zeolite powder (MOR)				
CBV 21A	20	Ammonium	0.08	500
Beta-zeolite powder (BEA)				
CP 814E	25	Ammonium	0.05	680
Ferrierite type zeolite powder (FER)				
CP 914C	20	Ammonium	0.05	400
ZSM-5-type zeolite powders (MFI)				
CBV 3024E	30	Proton	0.10	400
CBV 8014	80	Ammonium	0.05	425
CBV 28014	280	Ammonium	0.05	400

used.[73] The needed catalyst amount was put into the autoclaves while purging the whole system with argon. After the addition of the catalyst and DMM, the reactors were closed and purged three times with CO to remove residual air traces. The needed amount of CO was dispensed with high accuracy using a specific mass-flow-controller (±1 ml; Bronkhorst, EL-Flow Select). The whole plant was steered using a specific Graphic User Interface based on the HitecZang Labvision software, which is able to control all pneumatic valves, stirrers, heating mantles and to record working pressures and temperatures. All experiments could be conducted using pre-defined receipts with the HiBatch software, thus guaranteeing a high reproducibility of the results. Specific HiBatch receipts were used to maintain the desired pressure over several hours in the case of isobaric performed experiments. The amount of dispensed CO was systematically recorded over the course of the reaction in order to calculate the corresponding conversion.

3.2. Catalysts, analytics and test apparatus

3.2.1. Catalyst pre-treatment: calcination and catalyst drying. Different solid acid supports were used as received. All zeolites were calcined before use at 550 °C for 6 h (ramp: 1 h to 550 °C). Two kinds of solid acid catalysts were tested in this study and characterised: seven zeolites with different structural properties and different SiO_2/Al_2O_3 ratios and seven commercially available ion exchange resins were compared. For comparability purposes, all the ion exchange resins were dried for 12 h at 110 °C under reduced pressure ($p < 10$ mbar) before usage. A summary of all tested ion exchange resins is shown in Table 5.

Table 5 Overview of all tested ion exchange resins employed in this study

Ion exchange resin	Tradename	Supplier	Details
DX2	Dowex50WX2	Rohm & Haas	Mesh 200–400
DX4	Dowex50WX4	Rohm & Haas	Mesh 50–100
DX8	Dowex50WX8	Rohm & Haas	Mesh 50–100
A15	Amberlyst 15	Dow Chemical	—
A16	Amberlyst 16	Dow Chemical	—
A36	Amberlyst 36	Dow Chemical	—
A46	Amberlyst 46	Dow Chemical	—

3.2.2. Ion exchange resins as catalysts. In general, commercially available acidic ion exchange resins are sulfonated styrene–divinylbenzene copolymers with $-SO_3H$ as the acid group. The thermal stability region of all ion exchange resins is below 150 °C, which means that a controlled acid catalysis is only possible under mild reaction conditions. The structure of such catalysts is divided in gel-type resins (*e.g.* Dowex catalysts) and macroreticular resins (*e.g.* Amberlyst catalysts), depending on the procedure of the copolymerization with divinylbenzene (DVB).[51,74] Gel-type resins are styrene–DVB copolymers that do not show spaces between the polymer chains in the dry state, *i.e.* the possess only micropores. Macroreticular resins are copolymerized in the presence of a solvent, such as toluene. After removal of the solvent, the originally solvent-filled spaces become pores. Therefore, such macroreticular resins can be described as gel-phase microspheres dispersed in macropores.[55] The DVB content also has an influence in the morphology of the catalyst. The higher the crosslinker content, the more DVB units are linked to the styrene chains and therefore the stiffer the resin structure gets. The crosslinker backbone can limit the accessibility of the catalytic active sites. This structure changes depending on the medium in which the reaction occurs. Generally speaking, macropores are large pores with diameters $d > 50$ nm (ref. 75) and are permanently present in the catalyst. When using polar media (*e.g.* water or alcohols) in the reaction, the polymer of the catalyst may swell, leading to non-permanent micro- and mesopores (micropores: $d \leq 2.0$ nm; mesopores: 2.0 nm $< d \leq 50$ nm)[75] which can improve the accessibility to inner active centres. Especially strong polar solvents lead to an expansion of the polymer chains because of the repulsive interaction between the polar solvent and the non-polar crosslinked polymeric structure of the catalyst.[76] Using linear ethers usually does not lead to a swelling of the ion exchange resins.[51,53,54] Since the reaction occurs with DMM (*i.e.* OME_1), which belongs to the oxymethylene ether chemical class, there should not be a strong swelling effect to be accounted for. In addition, the higher the crosslinker content in the catalyst, the smaller is

Table 6 Summary of relevant features of employed ion exchange resins in this study

Ion exchange resin	Capacity (wet) [eq. l^{-1}]	Capacity (wet) [mol H^+ kg^{-1}]	Capacity (dry) [mol H^+ kg^{-1}]	Moisture[a] [%]	Density (wet)[a] [g l^{-1}]	Surface area [m^2 g^{-1}]	T_{max} [°C]	Company
Amberlyst 15	1.7[a]	2.21[b]	4.7[a]	52–57	770	53[a]	120[a]	Rohm & Haas
Amberlyst 16	1.7[a]	2.18[b]	4.8[a]	52–58	780	30[a]	130[a]	Rohm & Haas
Amberlyst 36	1.95[a]	2.44[b]	5.4[a]	51–57	800	33[a]	150[a]	Rohm & Haas
Amberlyst 46	0.8[a]	1.33[b]	0.43[a]	26–36	600	75[a]	120[a]	Rohm & Haas
Dowex 50WX2 (200–400 mesh)	0.6[a]	0.81[b]	3.68[b]	74–82	737	0.3[c]	150[d]	Dow Chemical
Dowex 50WX4 (50–100 mesh)	1.1[a]	1.43[b]	4.47[b]	64–72	769	0.3[c]	150[d]	Dow Chemical
Dowex 50WX8 (50–100 mesh)	1.7[a]	2.12[b]	4.51[b]	50–56	801	0.3[c]	150[d]	Dow Chemical

[a] Manufacturer's data. [b] Value derived from manufacturer's data. [c] Parameter measured by Oestreich.[82] [d] Value from Ramírez *et al.*[55]

the swelling effect; the swelling effect is more pronounced in gel-type resins and less with macroreticular resins.[51,52]

The acid catalytic activity of ion exchange resins is also markedly influenced by the degree of sulfonation of the polymer.[77–79] They are mostly stoichiometrically sulfonated, having one acid group per styrene or divinylbenzene monomer unit. Catalysts with a higher degree of sulfonation are called "persulfonated" resins and show stronger acid sites. This feature can be attributed to the structural interaction of neighbouring sulfonic acid groups, increasing the acid strength of the ion exchange catalyst.[77–79] In anhydrous media or media that do not induce swelling of the resins, the degree of sulfonation and the presence of sulfone bridges between the aromatic styrene are relevant structural features that determine the acid strength of the catalyst.[77–79] When using polar media, such as water, the ion exchange catalyst swells and can be described as a sulfonic acid solution within the gel-phase of the resin. With a higher degree of sulfonation, there is a higher concentration of sulfonic acid groups in the internal solution, increasing the strength of the acid groups, thus leading to a higher catalytic activity.[77–79] By employing aqueous or polar media that swell the resin, an enhancement of acid strength can be observed due on the one hand, to a high acid concentration in the gel-phase of the polymer, *i.e.* of the acid groups on the surface of the material,[77] and on the other hand to a higher accessibility to the active sites because of catalyst swelling.[51,80] Generally under non-aqueous conditions, the ion exchange resins have an acid strength comparable to an 63–70% aqueous H_2SO_4-solution and to a H-beta zeolite.[51,81]

A summary of relevant features of the ion exchange catalysts is presented in Tables 6 and 7.

In a direct comparison between the Amberlyst catalysts, A36 has the highest acidity, followed by A15, then A16 and finally A46 with the lowest acid concentration (see Table 6). However, A46 is sulfonated only at the catalyst surface, resulting in negligible amounts of acid sites in the gel phase of the polymer. As a result, all acid centres are present on the outer surface and therefore easily accessible for catalytic reactions. Furthermore, A46 has about twice the surface area of A16 and A36, while the surface area of A15 is average when compared to the other catalysts. With the highest pore diameter of 300 Å from A15, it has more easily accessible active centres than the other Amberlyst catalysts (with exception of A46 since it has almost all active sites on the outer polymer surface). In addition, A36 is an oversulfonated ion exchange resin, leading to higher acid capacity and acid strength, when compared to monosulfonated catalysts with the same DVB content.[51]

Regarding the crosslinker, a low DVB content usually leads to higher effects of swelling when using polar media in the reaction, creating nonpermanent micro- and mesopores which can enhance permeability of reactants.[51,52] However, this effect shall be considered negligible in the carbonylation of DMM, since linear ethers usually do not swell ion exchange resins.[51,53,54]

Further information for the catalysts of the Amberlyst series is described in Table 7.

3.2.3. BET measurements. Fig. 12 shows the adsorption–desorption curves for all of the seven zeolites and the summary of the evaluation is shown in Table 8. All zeolites exhibit a type IV isotherm, indicating the mesoporous character of the zeolites used in this study.[84] Beside the Y-30 and M-20 zeolite, all zeolites show a hysteresis loop and can therefore be attributed to the type IV a) isotherm, whereas the Y-30 and M-20 zeolites can be attributed to IV b) isotherms.[84] The surface area measurements show significant

Table 7 Further information on catalyst characteristics for the Amberlyst series (manufacturer's data)

Ion exchange resin	Particle size [mm]	Average pore diameter [Å]	Pore volume [$cm^3 \cdot g^{-1}$]	Divinylbenzene (DVB) content[a] [%]
Amberlyst 15	0.60–0.85	300	0.40	20
Amberlyst 16	0.60–0.80	250	0.20	12
Amberlyst 36	0.60–0.85	240	0.20	12
Amberlyst 46	n.a.	235	n.a.	25

[a] Value from Bringué *et al.*[51] and Ramírez *et al.*[83]

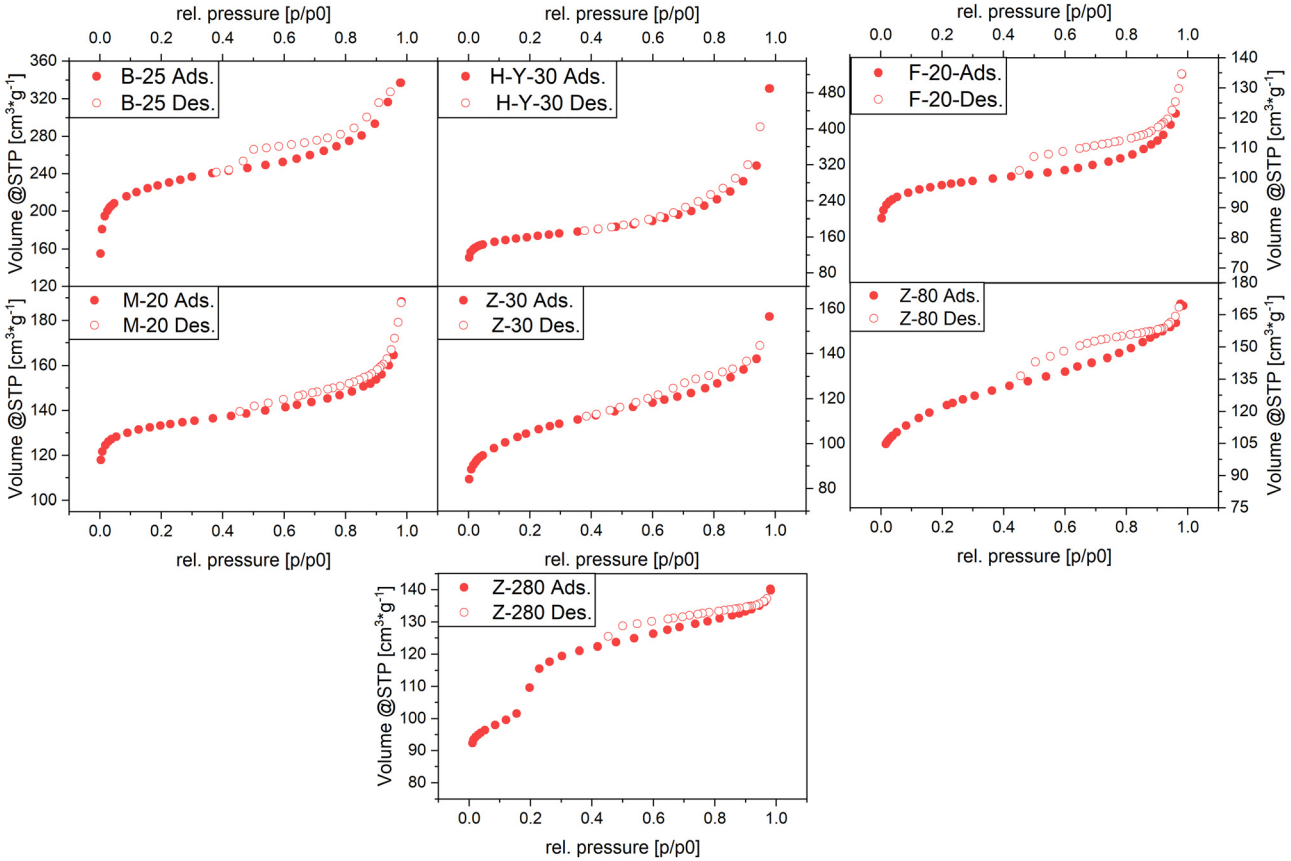

Fig. 12 BET adsorption–desorption curves for all seven tested zeolites (Ads. = Adsorption isotherm and Des. = Desorption Isotherm).

differences between the zeolites, B-25 and Y-30 zeolite exhibiting the highest surface area of all measured catalysts. Interestingly, these zeolites display a substantial difference in the ratio of external surface area to micropore area. Y-30 exhibits a lower external surface area compared to the B-25 zeolite. From all the other zeolites, the M-20 zeolite shows the lowest external surface area. This low external surface area is the main reason for the missing of the hysteresis loop for the M-20 and Y-30 zeolite. The lower limit of the desorption branch of all H4 hysteresis loop indicates the p/p_0 value at which cavitation takes place. The B-25, F-20 and Z-80 show this cavitation point when the relative pressure is around 0.5. During adsorption, the Z-280, which is the zeolite with the lowest acidity used in this study, shows a rather steep increase of adsorbed gas at a relative pressure between 0.2 and 0.3. This indicates the point at which pore condensation in the mesopores occurs. Beside the B-25 zeolite, all zeolites exhibit a similar pore diameter evaluated with the BJH method (Barrett, Joyner and Halenda[85]), with values ranging between 3.8 and 3.9 nm. B-25 is the only zeolite showing a pore diameter of 6.8 nm with a pore volume of 0.57 $cm^3\ g^{-1}$, meaning it has the highest pore volume and pore diameter. The pore volumes differ between the high surface area and low surface area zeolites. B-25 and Y-30 exhibit a higher surface area and also show one number of magnitude higher pore volumes than all the other zeolites.

Table 8 Summary of the evaluation of the BET measurements of the different zeolites

	MBET	*V–t* method summary (DeBoer)				BJH method		
Zeolite	Surface area [$m^2\ g^{-1}$]	Micropore volume [$cm^3\ g^{-1}$]	Micropore area [$m^2\ g^{-1}$]	External surface area [$m^2\ g^{-1}$]	Ratio external surface area to micropore area	Surface area [$m^2\ g^{-1}$]	Pore volume [$cm^3\ g^{-1}$]	Pore diameter [nm]
B-25	602	0.171	425	177	0.416	159	0.570	6.789
Y-30	879	0.297	744	134	0.180	115	0.204	3.896
F-20	391	0.140	364	27	0.074	28	0.065	3.830
M-20	537	0.188	496	41	0.083	27	0.091	3.863
Z-30	395	0.132	324	72	0.222	39	0.088	3.839
Z-80	458	0.150	362	95	0.262	46	0.076	3.859
Z-280	405	0.160	336	69	0.205	19	0.033	3.834

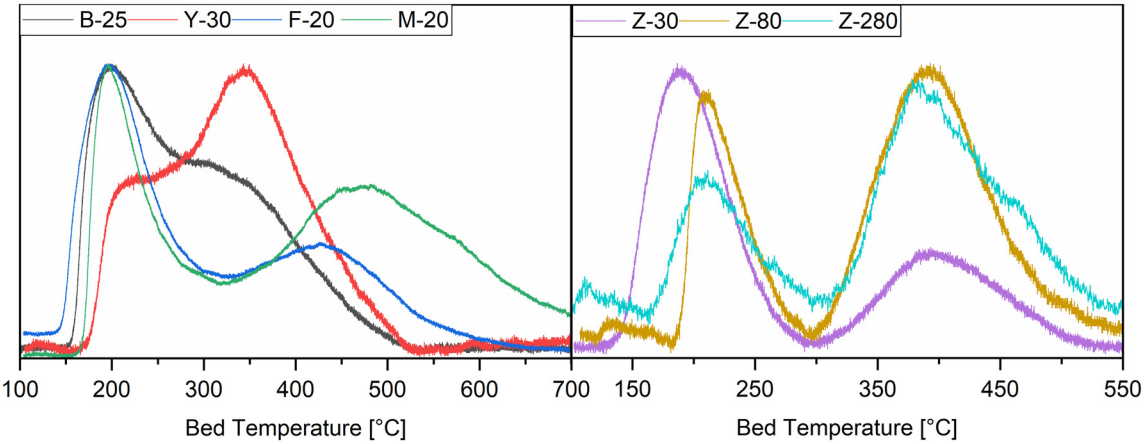

Fig. 13 Normed and baseline corrected thermograms obtained from NH_3-TPD measurements on all zeolites presented in this work.

Interestingly though, the Y-30 shows the same pore diameter than all the others, meaning the number of pores on this zeolite is the highest.

3.2.4. Temperature programmed desorption (TPD) measurements. The desorption behaviour of ammonia (NH_3) on zeolites is one of the most commonly used measurement techniques to characterise the acidity of such catalysts.[84] This method is a useful tool to distinguish between different acid sites, but the evaluation can be affected negatively because of re-adsorption phenomena, when desorbed ammonia is leaving the pores.[85] Other probe molecules are also discussed in the literature, but ammonia is the most commonly used gas because of its small molecule size and high basicity, thus being ideal to monitor a wide range of acid centres. Because of big structural differences between all tested zeolites, the range of thermograms and data obtained is vast (see Fig. 13). Generally, two desorption bands can be noticed for all zeolites. The low temperature desorption (LTD) of NH_3 measured in between 189–212 °C and the high temperature NH_3 desorption (HTD) measured between 326 and 482 °C. The LTD corresponds to weak acid site, while the second HTD corresponds to strongly adsorbed NH_3.[86] Categorising the acid sites in weak (100–250 °C), medium (251–350 °C), strong (351–450 °C) and very strong (450–600 °C) shows interesting relationships between the different zeolites. One can say that every zeolite has a distinct peak in the weak acid site region, beside the Y-30 zeolite, which shows only a shoulder in this region. Furthermore, only one distinct peak is measured in the very strong acid site region by the mordenite zeolite, indicating a very broad distribution of acidic strength ranging from medium to very strong acid sites. The F-20 zeolite also shows a very broad HTD also ranging from strong to very strong acid sites. Y-30 and B-25 nearly show symmetrical thermograms, whereas the B-25 thermogram has its highest peak at the LTD and the Y-30 at the HTD peak.

Assessing the peak surfaces and the related NH_3 uptakes allows additionally to evaluate the amounts of the different acidic centres in each zeolite (see Table 9). F-20 shows the highest NH_3 uptake meaning it has the highest acid density from all tested zeolites, whereas Z-280 being the zeolite with the lowest acidity (lower Al-content) shows an NH_3 uptake which is two orders of magnitude lower than that of the F-20 catalyst. Therefore, reducing the Al-content directly influences the acid density of zeolite catalyst, because Lewis and Brønsted acid centres are located in the vicinity of AlO_4 tetrahedrons in the zeolite structures.[87–91] After F-20, M-20 shows the second highest overall NH_3 uptake followed by B-25 and Z-30 which show very similar NH_3 uptakes. The second lowest uptake was measured for the zeolite with the second lowest Al-content, which is the Z-80 zeolite with only 317 μmol g^{-1}. By deconvolution of the raw data the percentage contribution of each peak to the overall NH_3 uptake can be calculated (details see ESI† Fig. S5). Nearly half of the overall high NH_3 uptake of the F-20 catalyst is related to weak acid sites, whereas the other half is distributed over strong and very strong acid sites. M-20, which also has a very high overall uptake, has a different distribution. Here, three quarters of the overall NH_3 uptake is provided by acid centres ranging from 320 to over 650 °C. Even though B-25 and Z-30 have very similar total NH_3 uptakes, the distribution of the acid centres is quite different. Three quarters of the B-25 NH_3 uptake can be attributed to medium and strong acid centres.

Table 9 Data obtained from NH_3-TPD measurements for the different zeolites used in this study. Desorption signals marked with "^{S}" are seen as shoulders in the thermograms. The values in brackets shows the percentage contribution of this peak to the overall NH_3 uptake. For details on how these values were calculated see ESI† Fig. S5

Zeolite	Low temp. Desorption [°C]	High temp. Desorption [°C]	NH_3 uptake [μmol g^{-1}]
B-25	199 (23%)	326^S (77%)	596.55
Y-30	211^S (14%)	347 (86%)	320.02
F-20	197 (44%)	427 (56%)	1065.80
M-20	196 (23%)	482 (77%)	836.15
Z-30	189 (65%)	393 (35%)	608.91
Z-80	210 (28%)	393 (72%)	317.07
Z-280	212 (25%)	382 (75%)	65.67

By contrast, nearly two thirds of the Z-30 uptake can be attributed to weak acid centres. The remaining one third of the Z-30 uptake is located in the strong to very strong acid sites range. Within the MFI zeolite range, Z-30 displays the highest NH_3 uptake while having the highest amount of weak acidic sites. In comparison, Z-80 and Z-280 have a similar NH_3 uptake distribution with one quarter in LTD and three quarters in HTD.

3.2.5. Gas chromatography. The liquid samples taken from the reactors were measured in an off-line GC (Agilent Technologies, GC8890) equipped with an auto sampler. Detailed information about the used method can be found in the ESI.† After withdrawing the liquid sample from the reactor and removing residual catalyst powder or beads, the freshly filtered samples were gathered in the auto sampler and promptly analysed. The relative concentrations of all products were calculated from the measured areas, after due calibration with a typical standard. The DMM conversion was calculated comparing with its area at the beginning of the reaction. All samples were injected three times to give a good estimate of the statistic error.

3.2.6. Physico-chemical and fuel properties. Melting point (ASTM D5972: 2016), refractive index (DIN 51423-2: 2010), surface tension (DIN EN 14370: 2004), flash point (DIN EN ISO 3679: 2015), autoignition point (DIN 51794: 2003), cetane number (DIN EN 17155: 2018), cold filter plugging point CFPP (DIN EN 116: 2018) and lubricity HFRR (DIN EN ISO 12156-1: 2019) of pure MMA were determined according to the certificated standard test methods performed by the certified company ASG Analytik-Service AG.

Additionally, heating value, density and kinematic viscosity were measured by in-house analytics. The density measurement was performed in a digital analyser DMA 4500 M from Anton Paar, consisting of a U-shaped oscillating sample tube, which is electronically excited to vibrate at its normal frequency. By precisely measuring the normal frequency and adjusting it appropriately, the density of the sample can be determined. The kinematic viscosity was measured using a Modular Compact Rheometer from Anton Paar. The time for a volume of liquid to flow under gravity through a calibrated cylindrical viscometer at 40 °C with rotational speed of 10 rpm was measured. The heating value was measured employing a C5003 calorimeter from IKA, with a C5001 cooling system, calibrated with benzoic acid under standard conditions.

4. Conclusions

This study investigated the reactivity of different solid acid catalysts for the carbonylation of DMM in the liquid phase without using an additional solvent. A catalyst screening with seven different zeolites and seven different ion exchange resins was performed. From the zeolites the Z-30 catalyst was the most active and from the ion exchange resins the A36 was the most active and selective catalyst. The ion exchange resins generally showed a completely different range in DMM conversion and MMA selectivity than the zeolite catalysts. Under the same circumstances, the ion exchange resin A36 showed a DMM conversion of 55% and a MMA selectivity of 96%, whereas the zeolite Z-30 showed a DMM conversion of 13% and a MMA selectivity of 32%.

For the zeolites, a low to moderate acid site density and a tendency for weak acid sites seems to be the best compromise for a moderate DMM conversion (13%) and MMA selectivity (36%), as seen in Z-30. The acid site density and strength seem to have a higher impact than accessibility of the pore structure.

For the ion exchange resins, the acid capacity and sulfonation degree are the most important catalyst properties to determine the product spectrum and conversion. This is especially the case because no swelling of the resins is expected, since linear ethers do not induce this phenomenon. Therefore, the crosslinker-content (divinylbenzene) does not play a major role in the reactivity of the carbonylation of DMM in the liquid phase.

The most active and selective catalyst found in this study was the ion exchange resin A36. Thus, this catalyst was used in a further parameter study analysing the effect of catalyst amount, temperature, pressure and reaction operation. The results from the parameter studies can be summarized as follows:

- The catalyst amount variation was performed with 0.5, 1.0 and 1.5 g catalyst at a temperature of 110 °C. From this study, 1.0 g was chosen as the ideal catalyst amount for further studies, because the reaction rate differs most from 0.5 g to 1.0 g but does not differ as much from 1.0 g to 1.5 g.
- The effect of temperature was analysed in a range of 40 to 140 °C after a reaction time of 4 h. At higher temperatures (>110 °C) a stronger catalyst deactivation and enhancement of the DME formation side reaction was observed. Therefore, 110 °C was chosen as the benchmark temperature for future studies.
- The pressure dependency of the catalytic activity of A36 was studied in a range between 20 and 80 bar. The highest conversion of DMM after 1 h was observed at 60 bar and increasing the pressure to 80 bar did not have a high impact in the CO or DMM conversion. In this study, at 20 bar, the amount of DMM being decomposed to DME and FA was the highest. FA is a couple product of DMM decomposition and undergoes the disproportionation reaction to MeFo, explaining the broader product spectrum at lower pressures.

In addition, the suitability of MMA as a diesel and gasoline substitute fuel was investigated by determining important physico-chemical and fuel properties. The measured fuel properties showed that MMA is unsuitable as a diesel fuel replacement. However, as an oxygenate, it still represents a possible diesel fuel additive, considering the soot and NOx reduction potential of a fuel blend, as well as good cold stability properties. Furthermore, with a low cetane number, MMA should present in turn a high octane number, resulting in a promising gasoline additive or substitute.

The liquid carbonylation of DMM presents complex side reactions, such as the formation of higher oxymethylene

ethers like OME_2, OME_3 and the carbonylation products of higher OME. However, by employing active and selective catalysts, such as A36 and improving reaction conditions, such as mild temperatures below 110 °C and moderate pressures at the range of 60 bar, a high MMA selectivity and educt conversion can be achieved. These findings can assist future attempts at a more efficient synthesis of MMA and therefore enable a scale-up of this process for industrial manufacturing as MMA shows many different applications in the fine chemical industry and fuel sector.

Abbreviations

A15	Amberlyst 15
A16	Amberlyst 16
A36	Amberlyst 36
A46	Amberlyst 46
ASTM	American Society for Testing and Materials
CFPP	Cold filter plugging point
DIN	Deutsches Institut für Normung
DMC	Dimethyl carbonate
DME	Dimethyl ether
DMM	Dimethoxymethane
DPF	Diesel particulate filter
DVB	Divinylbenzene
DX2	Dowex50WX2
DX4	Dowex50WX4
DX8	Dowex50WX8
EG	Ethylene glycol
EGR	Exhaust gas recirculation
FA	Formaldehyde
GC	Gas chromatograph
GC-MS	Gas chromatography – mass spectrometry
HC	Hydrocarbons
HFRR	High frequency reciprocating rig
MeFo	Methyl formate
MeOH	Methanol
MMA	Methyl methoxyacetate
n.a.	not available
NOx	Nitrogen oxides
OME	Oxymethylene ether
p	Pressure
p_{max}	Maximum pressure
PM	Particulate matter
Rel. conc.	Relative concentration
RON	Research octane number
SAC	Solid acid catalyst
SCR	Selective catalytic reduction
STP	Standard temperature and pressure
T, Temp.	Temperature
T_{max}	Maximum temperature
TPD	Temperature programmed desorption
WHO	World Health Organisation
X	Conversion
ZSM	Zeolite Socony Mobil

Author contributions

Conceptualization, K. A. S. and V. Z. F.; methodology, K. A. S.; software, K. A. S.; validation, K. A. S. and V. Z. F.; formal analysis, K. A. S. and V. Z. F.; investigation, K. A. S. and V. Z. F.; resources, J. S.; data curation, K. A. S. and T. A. Z.; writing—original draft preparation, K. A. S. and V. Z. F.; writing—review and editing, T. A. Z. and J. S.; visualization, K. A. S. and V. Z. F.; supervision, T. A. Z. and J. S.; project administration, J. S.; funding acquisition, J. S. All authors have read and agreed to the published version of the manuscript.

Conflicts of interest

There are no conflicts to declare.

Acknowledgements

The authors gratefully acknowledge financial support from the Bundesministerium für Bildung und Forschung (BMBF) within the NAMOSYN Project (FKZ 03SF0566K0). The authors also acknowledge the technical support of Ricki Drexler and the analytical support of Nikolaj Slaby and Doreen Neumann-Walter for the physisorption (BET) measurements.

Notes and references

1 A. Brown, T. B. Brown, A. Calabrese, D. Ellis, N. Puhalo, M. Ralph and L. Watson, Triazole oxytocin antagonists: Identification of an aryloxyazetidine replacement for a biaryl substituent, *Bioorg. Med. Chem. Lett.*, 2010, **20**, 516–520.
2 K. Takada, N. Imamura, K. R. Gustafson and C. J. Henrich, Synthesis and structure-activity relationship of botryllamides that block the ABCG2 multidrug transporter, *Bioorg. Med. Chem. Lett.*, 2010, **20**, 1330–1333.
3 N. Sakai, H. Hori, Y. Yoshida, T. Konakahara and Y. Ogiwara, Copper(I)-catalyzed coupling reaction of aryl boronic acids with N,O-acetals and N,N-aminals under atmosphere leading to α-aryl glycine derivatives and diarylmethylamine derivatives, *Tetrahedron*, 2015, **71**, 4722–4729.
4 H. Furukawa, Y. Miyamoto, Y. Hirata, K. Watanabe, Y. Hitomi, Y. Yoshitomi, J. Aida, N. Noguchi, N. Takakura, K. Takami, S. Miwatashi, Y. Hirozane, T. Hamada, R. Ito, M. Ookawara, Y. Moritoh, M. Watanabe and T. Maekawa, Design and Identification of a GPR40 Full Agonist (SCO-267) Possessing a 2-Carbamoylphenyl Piperidine Moiety, *J. Med. Chem.*, 2020, **63**, 10352–10379.
5 A. Suzuki, N. Fukuda, T. Kajiwara and T. Ikemoto, Practical Preparation of a 1,3,5-Trisubstituted Pyridazin-4(1 H)-one Using Selective C 1 Unit Insertion and Cyclization, *Org. Process Res. Dev.*, 2019, **23**, 484–492.
6 J. C. Adrian, J. L. Barkin, R. J. Fox, J. E. Chick, A. D. Hunter and R. A. Nicklow, Chlorotitanium enolate addition to aldimines: a stereoselective route to alpha-oxy-beta-substituted-beta-amino esters, *J. Org. Chem.*, 2000, **65**, 6264–6267.
7 L. Gooßen, M. Blanchot, M. Arndt and K. Salih, Synthesis of Botryllamides and Lansiumamides via Ruthenium-

Catalyzed Hydroamidation of Alkynes, *Synlett*, 2010, **2010**, 1685–1687.
8 A. L. Joffe, T. M. Thomas and J. C. Adrian, A stereoselective, multiple-component approach to α–β-substituted-β-amino carbonyl derivatives, *Tetrahedron Lett.*, 2004, **45**, 5087–5090.
9 L. K. Thalén and J.-E. Bäckvall, Development of dynamic kinetic resolution on large scale for (±)-1-phenylethylamine, *Beilstein J. Org. Chem.*, 2010, **6**, 823–829.
10 F. Balkenhohl, K. Ditrich, B. Hauer and W. Ladner, Optisch aktive Amine durch Lipase-katalysierte Methoxyacetylierung, *J. Prakt. Chem.*, 1997, **339**, 381–384.
11 V. Chandrashaker, M. Ptaszek, M. Taniguchi and J. S. Lindsey, Synthesis of diverse acyclic precursors to pyrroles for studies of prebiotic routes to tetrapyrrole macrocycles, *New J. Chem.*, 2016, **40**, 8786–8808.
12 M. Cammenberg, K. Hult and S. Park, Molecular basis for the enhanced lipase-catalyzed N-acylation of 1-phenylethanamine with methoxyacetate, *ChemBioChem*, 2006, **7**, 1745–1749.
13 D. Spasyuk and D. G. Gusev, Acceptorless Dehydrogenative Coupling of Ethanol and Hydrogenation of Esters and Imines, *Organometallics*, 2012, **31**, 5239–5242.
14 J. W. van Hal, J. S. Ledford and X. Zhang, Investigation of three types of catalysts for the hydration of ethylene oxide (EO) to monoethylene glycol (MEG), *Catal. Today*, 2007, **123**, 310–315.
15 B. Li, S. Bai, X. Wang, M. Zhong, Q. Yang and C. Li, Hydration of epoxides on CoIII(salen) encapsulated in silica-based nanoreactors, *Angew. Chem., Int. Ed.*, 2012, **51**, 11517–11521.
16 H. Yue, Y. Zhao, X. Ma and J. Gong, Ethylene glycol: properties, synthesis, and applications, *Chem. Soc. Rev.*, 2012, **41**, 4218–4244.
17 F. E. Celik, H. Lawrence and A. T. Bell, Synthesis of precursors to ethylene glycol from formaldehyde and methyl formate catalyzed by heteropoly acids, *J. Mol. Catal. A: Chem.*, 2008, **288**, 87–96.
18 H. Song, R. Jin, M. Kang and J. Chen, Progress in synthesis of ethylene glycol through C1 chemical industry routes, *Chin. J. Catal.*, 2013, **34**, 1035–1050.
19 M. Tamura, M. Ishino, T. Deguchi and S. Nakamura, A new catalyst for the direct synthesis of ethylene glycol from carbon monoxide and hydrogen, *J. Organomet. Chem.*, 1986, **312**, C75–C78.
20 D. R. Fahey, Rational Mechanism for Homogeneous Hydrogenation of Carbon Monoxide to Alcohols, Polyols, and Esters, *J. Am. Chem. Soc.*, 1981, **103**, 136–141.
21 S. E. Jacobson, Formaldehyde hydroformylation to glycol aldehyde via rhodium phosphine-amine and phosphine-amide catalysts, *J. Mol. Catal.*, 1987, **41**, 163–183.
22 Y. Sun, H. Wang, J. Shen, H. Liu and Z. Liu, Highly effective synthesis of methyl glycolate with heteropolyacids as catalysts, *Catal. Commun.*, 2009, **10**, 678–681.
23 Q. Shi, H. Guo, C. Chen, B. Hou, L. Jia and D. Li, An efficient Brønsted acidic polymer resin for the carbonylation of formaldehyde to glycolic acid, *React. Kinet., Mech. Catal.*, 2020, **130**, 1027–1042.
24 S. Y. Lee, J. C. Kim, J. S. Lee and Y. G. Kim, Carbonylation of formaldehyde over ion exchange resin catalysts. 1. Batch reactor studies, *Ind. Eng. Chem. Res.*, 1993, **32**, 253–259.
25 D. J. Loder, *US Pat.*, US2152852A, 1936.
26 F. Chen, L. Shi, J. Yao, Y. Wang, D. Zhang, W. Zhu and Z. Liu, A highly efficient sulfonic acid resin for liquid-phase carbonylation of dimethoxymethane, *Catal. Sci. Technol.*, 2018, **8**, 580–590.
27 F. Chen, L. Shi, S. Bello, J. Fan, Y. Wang, D. Zhang and J. Yao, Excellent prospects in methyl methoxyacetate synthesis with a highly active and reusable sulfonic acid resin catalyst, *New J. Chem.*, 2020, **44**, 1346–1353.
28 J. Wang, J. Liu, H. Song and J. Chen, Heteropolyacids as Efficient Catalysts for the Synthesis of Precursors to Ethylene Glycol by the Liquid-phase Carbonylation of Dimethoxymethane, *Chem. Lett.*, 2015, **44**, 806–808.
29 V. Shapovalov and A. T. Bell, Theoretical Study of Zeolite-Catalyzed Dimethoxymethane Carbonylation to Methyl Methoxyacetate, *J. Phys. Chem. C*, 2010, **114**, 17753–17760.
30 F. E. Celik, T.-J. Kim and A. T. Bell, Effect of zeolite framework type and Si/Al ratio on dimethoxymethane carbonylation, *J. Catal.*, 2010, **270**, 185–195.
31 G. Yanfeng, L. Shenghua, G. Hejun, H. Tiegang and Z. Longbao, A new diesel oxygenate additive and its effects on engine combustion and emissions, *Appl. Therm. Eng.*, 2007, **27**, 202–207.
32 X. Lü, J. Yang, W. Zhang and Z. Huang, Improving the Combustion and Emissions of Direct Injection Compression Ignition Engines Using Oxygenated Fuel Additives Combined with a Cetane Number Improver, *Energy Fuels*, 2005, **19**, 1879–1888.
33 D. Mei, K. Hielscher and R. Baar, Study on Combustion Process and Emissions of a Single-Cylinder Diesel Engine Fueled with DMC/Diesel Blend, *J. Energy Eng.*, 2014, **140**, 1–9.
34 B. Rajesh Kumar, S. Saravanan, B. Sethuramasamyraja and D. Rana, Screening oxygenates for favorable NOx/smoke trade-off in a DI diesel engine using multi response optimization, *Fuel*, 2017, **199**, 670–683.
35 J. Wang, F. Wu, J. Xiao and S. Shuai, Oxygenated blend design and its effects on reducing diesel particulate emissions, *Fuel*, 2009, **88**, 2037–2045.
36 W. Ying, L. Genbao, Z. Wei and Z. Longbao, Study on the application of DME/diesel blends in a diesel engine, *Fuel Process. Technol.*, 2008, **89**, 1272–1280.
37 H. W. Wang, L. B. Zhou, D. M. Jiang and Z. H. Huang, Study on the performance and emissions of a compression ignition engine fuelled with dimethyl ether, *Proc. Inst. Mech. Eng., Part D*, 2000, **214**, 101–106.
38 T. A. Semelsberger, R. L. Borup and H. L. Greene, Dimethyl ether (DME) as an alternative fuel, *J. Power Sources*, 2006, **156**, 497–511.
39 A. S. Cheng, R. W. Dibble and B. A. Buchholz, *The Effect of Oxygenates on Diesel Engine Particulate Matter*, 2002, DOI: **10.4271/2002-01-1705**.
40 Nanjing Joyin Pharmatech CO LTD, *China Pat.*, CN111004121A, 2020.

41 D. He, W. Huang, J. Liu and Q. Zhu, The activity of H4SiW12O40 for the coupling of formaldehyde and methyl formate to methyl glycolate and methyl methoxy acetate, *J. Mol. Catal. A: Chem.*, 1999, **145**, 335–338.
42 W. Huang, D. He, J. Liu and Q. Zhu, Catalytic condensation of formaldehyde and methyl formate over 12-tungstosilicic compounds, *Appl. Catal., A*, 2000, **199**, 93–98.
43 E. J. Strojny, R. T. Iwamasa and L. K. Frevel, Oxidation of 2-Methoxyethanol to Methoxyacetic Acid by Nitric Acid Solutions, *J. Am. Chem. Soc.*, 1970, 1171–1178.
44 S. D. Badmaev, D. I. Potemkin, A. A. Pechenkin, G. G. Volkova, V. A. Sobyanin and V. N. Parmon, Gas-phase carbonylation of dimethoxymethane to methyl methoxyacetate over the Cs2.5H0.5PW12O40 catalyst, *Dokl. Phys. Chem.*, 2016, **468**, 85–88.
45 F. E. Celik, T.-J. Kim and A. T. Bell, Vapor-phase carbonylation of dimethoxymethane over H-Faujasite, *Angew. Chem., Int. Ed.*, 2009, **48**, 4813–4815.
46 S. Liu, W. Zhu, L. Shi, H. Liu, Y. Liu, Y. Ni, L. Li, H. Zhou, S. Xu and Z. Liu, A highly efficient Nafion-H catalyst for vapour phase carbonylation of dimethoxymethane, *RSC Adv.*, 2014, **4**, 40999–41002.
47 J. Yao, Y. Wang, S. S. Bello, G. Xu and L. Shi, Regulation of Brønsted acid sites in H-MOR for selective methyl methoxyacetate synthesis, *Appl. Organomet. Chem.*, 2020, **34**, 1–9.
48 D. Zhang, L. Shi, Y. Wang, F. Chen, J. Yao, X. Li, Y. Ni, W. Zhu and Z. Liu, Effect of mass-transfer control on HY zeolites for dimethoxymethane carbonylation to methyl methoxyacetate, *Catal. Today*, 2018, **316**, 114–121.
49 F. E. Celik, T. Kim and A. T. Bell, *US Pat.*, US 2010/0105947 A1, 2008.
50 M. Drexler, P. Haltenort, U. Arnold and J. Sauer, Continuous Synthesis of Oxymethylene Ether Fuels from Dimethyl Ether in a Heterogeneously Catalyzed Liquid Phase Process, *Chem. Ing. Tech.*, 2022, **94**, 256–266.
51 R. Bringué, E. Ramírez, M. Iborra, J. Tejero and F. Cunill, Influence of acid ion-exchange resins morphology in a swollen state on the synthesis of ethyl octyl ether from ethanol and 1-octanol, *J. Catal.*, 2013, **304**, 7–21.
52 M. A. Tejero, E. Ramírez, C. Fité, J. Tejero and F. Cunill, Esterification of levulinic acid with butanol over ion exchange resins, *Appl. Catal., A*, 2016, **517**, 56–66.
53 R. Bringué, E. Ramírez, C. Fité, M. Iborra and J. Tejero, Kinetics of 1-pentanol Etherification without Water Removal, *Ind. Eng. Chem. Res.*, 2011, **50**, 7911–7919.
54 E. Medina, R. Bringué, J. Tejero, M. Iborra and C. Fité, Conversion of 1-hexanol to di-n-hexyl ether on acidic catalysts, *Appl. Catal., A*, 2010, **374**, 41–47.
55 E. Ramírez, R. Bringué, C. Fité, M. Iborra, J. Tejero and F. Cunill, Assessment of ion exchange resins as catalysts for the direct transformation of fructose into butyl levulinate, *Appl. Catal., A*, 2021, **612**, 117988.
56 A. Schultze-Jena, M. A. Boon, D. A. M. de Winter, P. J. T. Bussmann, A. E. M. Janssen and A. van der Padt, Predicting intraparticle diffusivity as function of stationary phase characteristics in preparative chromatography, *J. Chromatogr. A*, 2020, **1613**, 460688.
57 S. H. Ali and S. Q. Merchant, Kinetic Study of Dowex 50 Wx8-Catalyzed Esterification and Hydrolysis of Benzyl Acetate, *Ind. Eng. Chem. Res.*, 2009, **48**, 2519–2532.
58 J. Guilera, E. Ramírez, C. Fité, M. Iborra and J. Tejero, Thermal stability and water effect on ion-exchange resins in ethyl octyl ether production at high temperature, *Appl. Catal., A*, 2013, **467**, 301–309.
59 N. G. Polyanskii and P. E. Tulupov, Thermal Stability of Cation-exchange Resins, *Russ. Chem. Rev.*, 1971, **40**, 1030–1046.
60 K. A. Sheikh, T. A. Zevaco, J. Jelic, F. Studt and M. Bender, Efficient noble metal promoted bimetallic cobalt catalysts in the selective synthesis of acetaldehyde dimethyl acetal, *RSC Adv.*, 2023, **13**, 22698–22709.
61 J. Song, K. Cheenkachorn, J. Wang, J. Perez, A. L. Boehman, P. J. Young and F. J. Waller, Effect of Oxygenated Fuel on Combustion and Emissions in a Light-Duty Turbo Diesel Engine, *Energy Fuels*, 2002, **16**, 294–301.
62 L. Lautenschütz, D. Oestreich, P. Seidenspinner, U. Arnold, E. Dinjus and J. Sauer, Physico-chemical properties and fuel characteristics of oxymethylene dialkyl ethers, *Fuel*, 2016, **173**, 129–137.
63 A. Omari, B. Heuser, S. Pischinger and C. Rüdinger, Potential of long-chain oxymethylene ether and oxymethylene ether-diesel blends for ultra-low emission engines, *Appl. Energy*, 2019, **239**, 1242–1249.
64 S. Arias, J. R. Agudelo, A. Ramos and M. Lapuerta, Emissions from a Euro 6 engine using polyoxymethylene dimethyl ethers: Chemical effects vs mapping strategy, *Fuel*, 2023, **335**, 127017.
65 S. Mohankumar and P. Senthilkumar, Particulate matter formation and its control methodologies for diesel engine: A comprehensive review, *Renewable Sustainable Energy Rev.*, 2017, **80**, 1227–1238.
66 Y. R. Tan, M. Salamanca, J. Akroyd and M. Kraft, How do the oxygenated functional groups in ether, carbonate and alcohol affect soot formation in Jet A2 diffusion flames?, *Combust. Flame*, 2022, **243**, 111849.
67 Y. R. Tan, M. L. Botero, Y. Sheng, J. A. Dreyer, R. Xu, W. Yang and M. Kraft, Sooting characteristics of polyoxymethylene dimethyl ether blends with diesel in a diffusion flame, *Fuel*, 2018, **224**, 499–506.
68 Y. Viollet, J. Chang and G. Kalghatgi, Compression Ratio and Derived Cetane Number Effects on Gasoline Compression Ignition Engine Running with Naphtha Fuels, *SAE Int. J. Fuels Lubr.*, 2014, **7**, 412–426.
69 G. T. Kalghatgi, *Auto-Ignition Quality of Practical Fuels and Implications for Fuel Requirements of Future SI and HCC Engines*, 2005, DOI: **10.4271/2005-01-0239**.
70 T. Ryan and A. Matheaus, Fuel Requirements for HCCI Engine Operation, *Journal of Fuels and Lubricants*, 2003, **112**, 1143–1152.
71 P. Cox and A.-A. Tsochatzopoulos, *Directive 2003/17/EC of the European Parliament and of the council of 3 March 2003. amending Directive 98/70/EC relating to the quality of petrol*

and diesel fuels, The European Parliament and The Council of the European Union, 2003.

72 L. Lautenschütz, D. Oestreich, P. Haltenort, U. Arnold, E. Dinjus and J. Sauer, Efficient synthesis of oxymethylene dimethyl ethers (OME) from dimethoxymethane and trioxane over zeolites, *Fuel Process. Technol.*, 2017, **165**, 27–33.

73 K. A. Sheikh, R. Drexler, T. A. Zevaco, J. Sauer and M. Bender, Hydrogenation of Carbon Monoxide in the Liquid Phase: Influence of the Synthetic Methods on Characteristics and Activity of Hydrogenation Catalysts, *Catalysts*, 2023, **13**, 482.

74 K. Jeřábek, *Inverse Steric Exclusion Chromatography as a Tool for Morphology Characterization*, 1996, vol. 635, pp. 211–224.

75 D. H. Everett, Manual of Symbols and Terminology for Physicochemical Quantities and Units, Appendix II: Definitions, Terminology and Symbols in Colloid and Surface Chemistry, *Pure Appl. Chem.*, 1972, **31**, 577–638.

76 J. Yao, L. Shi, W. Deng, J. Fan, Y. Wang, W. Gao, D. Zhang, W. Zhu and Z. Liu, Facile sulfolane-modified resins for enhanced dimethoxymethane carbonylation, *Catal. Sci. Technol.*, 2020, **10**, 2561–2572.

77 M. Hart, G. Fuller, D. R. Brown, J. A. Dale and S. Plant, Sulfonated poly(styrene-co-divinylbenzene) ion-exchange resins: acidities and catalytic activities in aqueous reactions, *J. Mol. Catal. A: Chem.*, 2002, **182-183**, 439–445.

78 M. Hart, G. Fuller, D. R. Brown, C. Park, M. A. Keane, J. A. Dale, C. M. Fougret and R. W. Cockman, Acidities and catalytic activities of persulfonated poly(styrene-co-divinylbenzene) ion-exchange resins, *Catal. Lett.*, 2001, **72**, 135–139.

79 S. Koujout, B. M. Kiernan, D. R. Brown, H. Edwards, J. A. Dale and S. Plant, The Nature of the Internal Acid Solution in Sulfonated Poly(styrene-co-divinylbenzene) Resins, *Catal. Lett.*, 2003, **85**, 33–40.

80 P. F. Siril, H. E. Cross and D. R. Brown, New polystyrene sulfonic acid resin catalysts with enhanced acidic and catalytic properties, *J. Mol. Catal. A: Chem.*, 2008, **279**, 63–68.

81 R. Bringue, M. Iborra, J. Tejero, J. Izquierdo, F. Cunill, C. Fite and V. Cruz, Thermally stable ion-exchange resins as catalysts for the liquid-phase dehydration of 1-pentanol to di-n-pentyl ether (DNPE), *J. Catal.*, 2006, **244**, 33–42.

82 D. Oestreich, *PhD*, Karlsruher Institut für Technologie (KIT), 2017.

83 E. Ramírez, R. Bringué, C. Fité, M. Iborra, J. Tejero and F. Cunill, Role of ion-exchange resins as catalyst in the reaction-network of transformation of biomass into biofuels, *J. Chem. Technol. Biotechnol.*, 2017, **92**, 2775–2786.

84 D. P. Ivanov, A. S. Kharitonov and L. V. Piryutko, Phenol oxidation by nitrous oxide: The role of zeolite catalyst acidity, *Catal. Ind.*, 2015, **7**, 275–281.

85 J. Cejka, A. Corma and S. Zones, *Zeolites and Catalysis. Synthesis, Reactions and Applications*, Wiley-VCH, Weinheim, 2010.

86 J. Zhang, P. Cao, H. Yan, Z. Wu and T. Dou, Synthesis of hierarchical zeolite Beta with low organic template content via the steam-assisted conversion method, *Chem. Eng. J.*, 2016, **291**, 82–93.

87 J. Weitkamp, Zeolites and catalysis, *Solid State Ionics*, 2000, **131**, 175–188.

88 M. Jin, M. Ravi, C. Lei, C. J. Heard, F. Brivio, Z. Tošner, L. Grajciar, J. A. van Bokhoven and P. Nachtigall, Dynamical Equilibrium between Brønsted and Lewis Sites in Zeolites: Framework-Associated Octahedral Aluminum, *Angew. Chem.*, 2023, **135**, 1–6.

89 J. Brus, L. Kobera, W. Schoefberger, M. Urbanová, P. Klein, P. Sazama, E. Tabor, S. Sklenak, A. V. Fishchuk and J. Dědeček, Structure of framework aluminum Lewis sites and perturbed aluminum atoms in zeolites as determined by 27Al{1H} REDOR (3Q) MAS NMR spectroscopy and DFT/molecular mechanics, *Angew. Chem., Int. Ed.*, 2015, **54**, 541–545.

90 C. Schroeder, M. R. Hansen and H. Koller, Ultrastabilization of Zeolite Y Transforms Brønsted-Brønsted Acid Pairs into Brønsted-Lewis Acid Pairs, *Angew. Chem., Int. Ed.*, 2018, **57**, 14281–14285.

91 B. Xu, C. Sievers, S. Hong, R. Prins and J. Vanbokhoven, Catalytic activity of Brønsted acid sites in zeolites: Intrinsic activity, rate-limiting step, and influence of the local structure of the acid sites, *J. Catal.*, 2006, **244**, 163–168.